LBL-21780
Preprint

Lawrence Berkeley Laboratory
UNIVERSITY OF CALIFORNIA

Submitted to Nuclear Physics A

HIGH-SPIN STATE SPECTROSCOPY IN ^{165,166}Yb

E.M. Beck, J.C. Bacelar, M.A. Deleplanque,
R.M. Diamond, F.S. Stephens, J.E. Draper,
B. Herskind, A. Holm, and P.O. Tjøm

June 1986

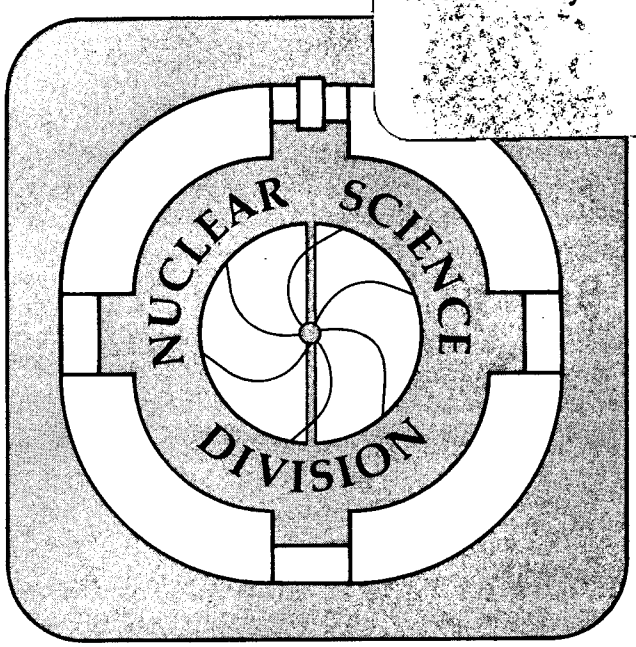

Prepared for the U.S. Department of Energy under Contract DE-AC03-76SF00098

DISCLAIMER

High-spin State Spectroscopy in $^{165, 166}$Yb

E.M. Beck, J.C. Bacelar, M.A. Deleplanque, R.M. Diamond and F.S. Stephens

Nuclear Science Division, Lawrence Berkeley Laboratory, University of California, Berkeley, CA 94720, U.S.A.

J.E. Draper

University of California, Davis, CA 95616, U.S.A.

B. Herskind and A.Holm

The Niels Bohr Institute, University of Copenhagen, DK 2100 Copenhagen, Denmark

and

P.O. Tjøm

Physics Institute, University of Oslo, Oslo, Norway

E

NUCLEAR REACTIONS ^{130}Te(^{40}Ar,xn), E=180 MeV; measured E_γ, $\gamma\gamma\gamma$- coin, $\gamma(\theta)$.

^{165}Yb, ^{166}Yb deduced levels, J, π, rotational bands. Enriched targets.

High-spin State Spectroscopy in $^{165, 166}$Yb

E.M. Beck, J.C. Bacelar, M.A. Deleplanque, R.M. Diamond and F.S. Stephens

Nuclear Science Division, Lawrence Berkeley Laboratory, University of California, Berkeley, CA 94720, U.S.A.

J.E. Draper

University of California, Davis, CA 95616, U.S.A.

B. Herskind and A.Holm

The Niels Bohr Institute, University of Copenhagen, DK 2100 Copenhagen, Denmark

and

P.O. Tjøm

Physics Institute, University of Oslo, Oslo, Norway

Abstract

Level schemes of ^{165}Yb and ^{166}Yb are studied up to high spins. Triple γ-ray coincidence spectra are analyzed for the first time, and their usefulness is discussed. The observed bands in both nuclei are interpreted in terms of the cranked-shell model. In particular, the continuation of the lowest $i_{13/2}$ single quasineutron aligned band beyond the first observed backbend is seen in an odd-N nucleus and the interaction strength between this band and the three-quasiparticle band is evaluated. Constancy of the moment of inertia in ^{166}Yb is observed at high spins and interpreted.

1. Introduction

With the advent of Compton-suppressed multi-detector arrays a wealth of high quality $\gamma\gamma$ coincidence data has become available[1-5] and has promoted an explosive development in high-spin spectroscopy. It is now possible experimentally to follow the "cold" (near yrast) pathways of a nucleus while it deexcites from about spin 40$\hbar$ to the ground-state in many rare-earth nuclei. Thus the many interesting effects caused by large rotational frequencies can be studied with high precision. The Coriolis force causes the nucleus to align particles in order to build up angular momentum. The resulting "backbends"[6] or "upbends" have been understood now for more than ten years.[7] The frequency at which this alignment occurs and the amount of angular momentum gained are related to the j-value of the particles and the position of the Fermi level. Most recently the interplay between the aligned (quasi-) particles and the shape of the nucleus has been studied experimentally, yielding valuable information for the understanding of nuclear structure at high spins.[3,8,9]

Considerable effort has gone into the high-spin spectroscopy of ytterbium nuclei recently[10-14], which makes it one of the best studied isotope chains. In this article we study the two well deformed ytterbium isotopes ^{165}Yb and ^{166}Yb at high spins. With the Berkeley High-Energy-Resolution Array, HERA, it was possible to require a triple (or higher fold) Compton-suppressed γ coincidence for an event to be accepted. (See section 2.1.) The analysis of these triple events and their usefulness for discrete-line spectroscopy of well-deformed nuclei will be discussed in the following section, where the experimental results are presented. In sections 3.1. and 3.3. we discuss the two nuclei studied in this article in the framework of the cranked-shell model. In section 3.2. the evaluation of the interaction strength between the lowest $i_{13/2}$ single quasineutron aligned band

and the first band crossing it is given, based on the observed γ-ray branching. The moment of inertia of ^{166}Yb is discussed in section 3.4. Finally, section 4 summarizes the results of the analysis.

2. Experimental technique and analysis

2.1. Experimental technique

High-spin states in ytterbium isotopes were populated by means of the reaction ^{130}Te(^{40}Ar,4n-6n) $^{166\text{-}164}$Yb at a beam energy of 180 MeV, the beam being provided by the Lawrence Berkeley Laboratory 88-inch cyclotron. Triple and higher γ-coincidence data were recorded on magnetic tape from the HERA array[15], which consisted of 20 Compton-suppressed germanium detectors at that time. The requirement of at least three Compton-suppressed γ rays in coincidence discriminates efficiently against lower multiplicity processes such as Coulomb excitation and radioactivity. Approximately 90 x 10^6 triple or higher multiple events were registered using two thin, stacked targets of about 0.3 mg/cm^2, and 210 x 10^6 events were recorded using a thick target of about 1 mg/cm^2 on 13 mg/cm^2 gold-foil. The 5n channel (^{165}Yb) was the strongest, populated with a reaction yield of 39%, ^{166}Yb yielding 31%, and ^{164}Yb, 30%. We concentrated on high-spin spectroscopy of ^{165}Yb and ^{166}Yb since the 6n product ^{164}Yb had a low average input angular momentum. As the detectors are at eight different angles to the beam, angular correlation information was used to establish the multipolarity of the new γ-ray transitions where intensities permitted.

2.2. Triple-coincidence analysis

As this was the first experiment in which triple and higher multiple coincidence events were recorded with appreciable statistics, new methods of analysis were examined. The most obvious analysis was to break the events into ordinary "double" $\gamma\gamma$ coincidences, each triple giving three statistically independent doubles, each quadruple creating six independent doubles and so forth.*) By this procedure we obtained two-dimensional $\gamma\gamma$ coincidence spectra, a "doubles" (symmetrized) matrix, with 370 x 10^6 coincidences (from 100 keV to 1800 keV) for the unbacked experiment and with 920 x 10^6 coincidences for the backed experiment, which we will refer to as full matrices. The first analysis of the data was performed using these matrices. For the highest-spin states, analysis of only the unbacked data could be used, because the lines above ≈ 800 keV suffer Doppler-broadening due to lifetimes plus feeding-times of the order of the mean slowing-down time for the recoiling nuclei in the gold backing (0.6 picoseconds). The two-dimensional spectrum of the backed data was extremely useful, however, in the analysis of the discrete γ-lines from the lower-spin states, as this matrix had better statistics by a factor of almost three and the "stopped" lines were sharper in resolution than the lines from the unbacked target.

A first step in the use of the triple-coincidence events was then taken. Each γ ray in the event was tested against a set of discrete-line gates belonging to a single product nucleus and, if within any gate limits, the coincident γ rays were treated as "doubles" and stored in an $E_{\gamma 1}$-$E_{\gamma 2}$ correlation matrix, which we will call "gated matrix". (For this purpose quadruple or higher multiple events were

---

*) From a n-tuple event n(n-1)/2 independent doubles are created.

first transformed into "triples".) The first γ ray thus served to select the product nucleus and to enhance the photopeak-to-background ratio. A selection of gates in ^{165}Yb and in ^{166}Yb, as well as a set of background gates, were used to increment three such matrices. Gates on transitions common to two or more of the three ytterbium isotopes produced in the reaction were not included. The background matrix to be subtracted from the matrices in coincidence with the 4n and 5n gates was scaled to the total background area underneath the discrete-line peaks in these gates. Total projections of the ^{165}Yb and ^{166}Yb gated matrices after subtraction of such an appropriate background matrix are shown in fig. 1, together with the total projection of the full "doubles" matrix of the unbacked data set. The reaction channel selection in the first two spectra is remarkable; the amount of 4n in the ^{165}Yb matrix, and 5n in the ^{166}Yb matrix, is reduced considerably and the 6n channel is strongly suppressed in both matrices. The remaining contaminants are due to a choice of gatewidth not restrictive enough. Also the peak-to-background ratio is improved by a factor of three for energies above 450 keV in the projection derived from the gated matrices compared with that from the full matrix, while the absolute background is lowered by a factor of about twenty.
Of course this selectivity comes with a loss in statistics: The photopeaks derived from the gated matrix for ^{165}Yb contain about one tenth the number of counts in the photopeaks from the full matrix, and for ^{166}Yb about one seventh the number. However, if one looks at spectra gated by high-spin transitions, there is only a loss of a factor of seven in statistics for ^{165}Yb and of four for ^{166}Yb for the photopeaks above the gate in comparison with the same gates from the full matrix, because of the better peak-to-background ratio in the gated matrices. To illustrate this point, the two spectra in fig. 2 are in coincidence with the same 490 keV gate, one taken in the full (top) and one in the gated matrix derived from ^{165}Yb lines (bottom). The structure of the (-,+1/2) band in ^{165}Yb is clearly visible in the double-gated spectrum, whereas the single-gated spectrum looks confusing because of strong contamination by the 6n reaction channel. The loss in statistics of the gated matrices is partially compensated by the cleanliness of these matrices; a whole series of

gates, in one band for example, can be summed in contrast to the case of the full matrix where typically only about three gates are sufficiently clean to sum. (See fig. 3, 4, 5.) Whether the selectivity and simplicity obtained in these spectra compensates for the loss of statistics depends on the number and intensity of the photopeaks chosen as gates to create the matrix. In our case, the derived ^{165}Yb matrix was obtained by 19 gates (equivalent to 18 % of the total feeding of the nucleus) resulting in 16 million counts from 100 keV to 1200 keV in the background-subtracted matrix, and the ^{166}Yb matrix came from 35 gates (equivalent to 23 % of the total feeding of the nucleus) resulting in 17 million counts.

The recording of triple and higher multiple events furthermore offers new perspectives for the analysis of energy correlations. The good statistics available make it possible to look at the continuum γ rays in coincidence with a particular gate including a distribution of states (frequency slices) enabling the measurement of correlation widths and strengths.[16-18]) The possibilities in the use of triple- and higher-coincidence spectra for continuum studies are just beginning to be explored, and certainly much more sophisticated analyses will be developed in the near future.

2.3. Angular correlation analysis

The angular correlation information was obtained by creating a two-dimensional spectrum from the unbacked data with the γ rays in the six detectors close to 90^{o} on the y-axis and those in the eight detectors close to 40^{o} and 150^{o} on the x-axis. The statistics of this matrix are lower by a factor of four, relative to the full data set. If one compares projections of the same discrete-line gate onto the

x (40^o detectors) and y (90^o detectors) axes, a γ-ray transition of the same multipolarity and spin change as the gate has equal intensity in both projections, whereas those with different character are, in general, not the same. For instance, gating on a stretched quadrupole transition, a stretched dipole transition will be about twice as intense in the y projection, when the dipole is at 90^o and the gate is at 40^o, than in the x projection with the quadrupole gate at 90^o.[3,19] That is, the ratio I_{90o}/I_{40o} is expected to be one for a stretched quadrupole transition and about two for a stretched dipole transition, when the gate is a stretched quadrupole transition. Here, the subscript stands for the angle of the projected detectors.

2.4. Level scheme of ^{165}Yb

The decay sequences of ^{165}Yb were recently studied[10], the yrast band being observed up to $61/2^-$. We were able to add two or more transitions on top of each previously known band. The level scheme obtained from this experiment is depicted in fig. 6. The band-crossing transitions at lower spins are partly taken from ref. 10. Energies in brackets indicate that the transitions are tentative, spins in brackets indicate that we were not able to measure angular correlations due to the weakness of the transition itself or contamination by another transition of the same energy. In these cases our spin assignments are based on systematics and intensity arguments only.

We confirm the three transitions of 815 keV, 832 keV and 864 keV which were placed above the 728 keV $41/2^+ \rightarrow 37/2^+$ transition in a previous analysis.[10] However, we favor a reversed order between the 815 keV and 832 keV transitions, based on their intensities in gated spectra. Our

angular correlation ratios show clearly that the 832 keV transition is a quadrupole. The 815 keV transition is consistent with a quadrupole, although the multipolarity of this transition is hard to determine because of statistical fluctuations; the presence of a second 815 keV transition in the $(+,1/2)_2$*) band restricts the possible gates to the weak ones above the band-crossing. For the 864 keV transition and the ones preceding it our data indicate quadrupole character. Fig. 3c) shows the $(+,1/2)_1$ band and the new transitions above it. We observe a 1022 keV transition "feeding" the $33/2^+$ state of the $(+,1/2)_1$ band in addition to the reported 880 keV transition "feeding" the $37/2^+$ state of this band. We have evidence for the 577 keV and 533 keV transitions making the 880 keV and 1022 keV transitions cross-band transitions from the $(+,1/2)_2$ band to the $(+,1/2)_1$ band. Unfortunately these two energies correspond to strong transitions in ^{164}Yb (530 keV, 532 keV, 533 keV, 577 keV)[10]) rendering a positive assignment in ^{165}Yb difficult, since any imperfect background subtraction creates a tiny amount of ^{164}Yb peaks in the projected spectrum, and the peaks of interest have an intensitiy of the order of a percent of the $21/2^+ \rightarrow 17/2^+$ transition in ^{165}Yb only. In addition, we find a 680 keV (quadrupole) cross-band transition, tying the $45/2^+$ state of the $(+,1/2)_1$ band to the $(+,1/2)_2$ band. It seems unlikely that all of these transitions fit together within a keV accidentally. The presence of a second 680 keV transition "feeding" the $33/2^+$ state of the $(+,1/2)_1$ band directly is not clear.

---

*) A decay sequence is labeled by the quantum numbers parity and signature $(\pi, \alpha)_n$ in accordance with the established convention, where n indicates the nth configuration of this type.[20])

The positive-parity three-quasiparticle band $(+,+1/2)_2$ band was extended up to spin $69/2^+$. Fig. 3b), which shows the $(+,+1/2)_2$ band, is the sum of six double-gated spectra derived from the ^{165}Yb gated matrix. The gates were chosen to be the 728.4 keV transition and the five preceding transitions in order to show the band structure without the contamination from the other bands which feed in at lower spins.

The negative-signature band (+,-1/2) was extended up to spin $47/2^+$. The (-,-1/2) band was extended up to spin $67/2^-$, which is shown in fig. 3d). This spectrum is again the sum of several double-gated spectra derived from the ^{165}Yb matrix. The negative-parity band (-,+1/2), which becomes yrast at high spins, was extended up to spin $77/2^-$. A typical double-gated spectrum, which is the sum of fourteen individual background-subtracted spectra derived from the ^{165}Yb gated matrix, is shown in fig. 3a).

Table 1 gives a summary of the experimental results for ^{165}Yb. The intensities were mostly taken from gated spectra because the presence of many interfering transitions in ^{164}Yb and ^{166}Yb made it impossible to use the total projection of the full "doubles" matrix. For the $I_{90}o/I_{40}o$ ratios (c.f. section 2.3) we used spectra in coincidence with known stretched quadrupole transitions and summed as many gates as possible in order to increase the statistics. Although the uncertainties for this ratio are typically 15 %, the distinction between stretched dipole and quadrupole transitions is clear.

2.5. Level scheme of ^{166}Yb

From previous studies the level scheme of ^{166}Yb was known up to spin 24^+ in the yrast band and to spin 22^- and spin 23^- in the negative-parity side bands respectively.[11] The level scheme which we extracted from the present data is given in fig. 7. The low-energy part of the scheme is partially taken from ref. 11, since we did not observe the γ-vibrational band based on the 2^+ state at 932 keV nor some other weak transitions in the lower part of the level scheme. As in the level scheme of ^{165}Yb, brackets are used to indicate that a transition or spin assignment is tentative.

Three transitions were added to the ground-state band extending it to spin 24^+. Angular correlation measurements could not be made individually for the three transitions which are close in energy. Therefore we summed the peak intensities for the three transitions and obtained a value $I_{90°}/I_{40°}$ in agreement with stretched quadrupole character. Fig. 4 is an example of the backed-target data showing the continuation of the ground-state band beyond the first backbend. The yrast band was extended up to spin 38^+. Fig. 5a) displays a typical spectrum, which was used for the construction of this band in the level scheme. The spectrum is a sum of ten background-subtracted double-gated spectra derived from the ^{166}Yb matrix. The (-,1) band was extended up to spin 37^-. Fig. 5b) shows a sum of high-spin gates in this band. Fig. 5c) shows the extension of the $(-,0)_1$ band up to spin 32^-.

We could also extend the band which has a bandhead at 1835 keV up to spin 26. Even spins and negative parity (as assumed in references 11,12) seem most likely for this band, though this is by no means certain. We were not able to measure angular correlation ratios, since the band is weakly populated (2% to 3% of the $6^+ \rightarrow 4^+$ ground-band transition) and all interband transitions

connecting the band with states of known spin and parity are hidden by strong quadrupole transitions of the same or very close-lying energies in ^{166}Yb, a problem which was previously reported.[11]) It is an interesting feature of this band, that its feeding pattern is very different from the other observed bands in ^{166}Yb. In the former the intensity gathered in the band stays practically constant throughout all the observed transitions, while in the latter up to 50 % of the intensity of a particular state is fed from the quasicontinuum.

Table 2 summarizes the information on ^{166}Yb obtained in the present experiment. The intensities and angular correlations were measured the same way as for ^{165}Yb.

3. Discussion

Rotational properties of high-spin states in well-deformed nuclei are usually interpreted in terms of cranked-shell-model (C.S.M.) calculations. For that purpose, the experimental excitation energies are transformed to the corresponding energies in a rotating frame of reference.[20]) To complete the analogy with model calculations, the contributions of the rotating core (reference configuration) are subtracted from the experimental data.[21]) Excitation energies (Routhians) and angular momenta (relative alignments) which are then measured are attributed to specific contributions from the available valence orbitals.

The effect of pairing correlations and Coriolis forces on the population of these orbitals has been investigated extensively during the past few years, and a wealth of information has been extracted. The decrease of the pairing correlations by blocking different orbitals was measured to be state dependent,[22]) and in some cases, evidence shows that a few orbitals could effectively reduce the pairing correlations to a negligible value.[3,13]) Lately the deformation-driving strengths of valence neutron and proton orbitals have been extremely important in the study of shape changes in the transitional region ($N \approx 88 - 90$)[3,8,23]) and of the loss of collectivity in heavier, well-deformed rare earths (^{166}Yb).[24]) At the very highest spins, a smooth behavior of certain quantities (I_x and moments of inertia) is generally observed in well-deformed rotors.[1])

We will discuss the quasiparticle states in ^{165}Yb and ^{166}Yb and their evolution to high spins in terms of Routhians and alignments.

3.1. Alignments in ^{165}Yb

The interpretation of the lower-frequency parts of the observed bands in terms of aligned quasiparticles has been given in previous studies.[10,25] The experimental Routhians of the bands in ^{165}Yb are shown in fig. 8. We choose a constant-moment-of-inertia reference, $\Im = 73\ \hbar^2\ \mathrm{MeV}^{-1}$, corresponding to a deformation $\beta = 0.24$.[10] With this reference, the Routhians are approximately parabolas whose curvature varies inversely with the moment of inertia of the band. The three-quasiparticle states have smaller curvature, since there was a large increase in the moment of inertia, associated with the decrease in the pairing correlations. The $(+,1/2)_1$ band is built on the lowest-lying positive-parity neutron orbital A*), and crosses the three-quasineutron aligned band ABC (open squares) at a frequency $\hbar\omega \approx 0.36$ MeV (BC alignment frequency). In this band the strong AB alignment is blocked, since the A quasiparticle state is occupied. Several additional states form a continuation of the $(+,1/2)_1$ band (see fig. 8, full squares), that is, are a continuation of A above the BC crossing frequency. To our knowledge, the continuation of an $i_{13/2}$ quasineutron aligned band beyond the BC crossing has not been observed previously in an odd-N nucleus. (This possibility has been suggested by ref. 27.) The negative-parity band (-,1/2), which becomes yrast above spin 53/2, is built on the orbital E and crosses EAB at $\hbar\omega \approx 0.23$ MeV (AB alignment frequency).[25] The (-,-1/2) band, built on F, is only observed above the AB alignment as the three-quasineutron aligned band, FAB.

---

*) In this notation A, B, C, D are the lowest unique-parity single-particle orbitals ($i_{13/2}$ neutrons for this neutron number) in the cranking model. E and F are the lowest two natural-parity orbitals (derived from the $h_{9/2}$ and $f_{7/2}$ neutrons for this neutron number).[26]

This is a common feature of the FAB band when nuclei are populated at very high spins (see ^{163}Er for one case where this band is known all the way to its band-head[9]). The (+,-1/2) band is built on the single-quasineutron state B. Therefore again as with the A band, the AB alignment is blocked.

In fig. 9 spin I is plotted versus rotational frequency $\hbar\omega$ for all bands in ^{165}Yb. In the continuation of the $(+,1/2)_1$ band an alignment appears to take place. One would expect it to be caused by the alignment of the positive-parity neutron orbitals C and D. However, there is no evidence for a band crossing at the same frequency in the two negative-parity bands, where it should also occur. The same type of contradiction arises if an EF alignment is assumed to be responsible, for then it should be observable in the three-quasiparticle band ABC also. However, the absence in the other bands of the band crossing possibly observed in the continuation of the A band can be understood if one assumes that the alignment of three quasineutrons reduces the neutron pairing correlations to such an extent, that the marked alignment of two more quasineutrons is not likely. In contrast, it is observed in the continuation of the A band, which has only a single aligned quasineutron, and much stronger pairing correlations exist. A possible bandcrossing in the B band at the highest observed spins may be with the BAD band, which is blocked in all other bands. Since the B band is weakly populated at higher spins, no information about alignments at higher frequencies (where the above discussed alignment in A occurs) is available.

Upbending is observed in the EAB band (yrast at high spins) for the very highest spin states, and the ABC band may show the start of upbending at the same frequency with its highest transition. We interpret this tentatively as the alignment of a pair of protons (probably the $i_{13/2}$ or $h_{9/2}$ orbitals), since they are expected to align around these frequencies.

3.2. Interaction strength of the BC crossing in ^{165}Yb

As all four levels closest to the crossing of the two interacting bands, A and ABC, are known, a first estimate of the strength of the interaction matrix element can be made by considering the energy differences between the levels of equal spin. The interaction matrix element is equal to or smaller than half the difference in energy of the two levels of the same spin.[28]) Thus, one finds an upper limit of $V < 52$ keV for the interaction strength between the A and ABC bands in ^{165}Yb.

We proceed to evaluate the interaction matrix element by means of the four-level scheme depicted in fig. 10.[28,29]) We assume the interaction to be proportional to I, mixing only states of the same spin. Then the Hamiltonian can be diagonalized (and should give the experimental energies). However, the system is only uniquely determined if we have one more condition for the unknowns. We use the branching ratio from state I to the two states of spin I-2, where the same rotational E2 matrix element is assumed within the two bands and the matrix element between the unperturbed bands is neglected. The relative transition rates from, e.g., the lower level of spin $I=45/2^+$ to the upper and lower levels of spin I-2 are determined experimentally. We obtain the following equations:

$$\tan(2x) = \frac{2V}{-\sqrt{(E_1-E_2)^2+(2V)^2}}$$

$$\tan(2y) = \frac{2V\,(I-2)/I}{\sqrt{(E_3-E_4)^2+[2V(I-2)/I]^2}}$$

$$\cot^2(x-y) = \frac{B(E2;I'\rightarrow I-2)}{B(E2;I'\rightarrow I'-2)}$$

where x and y determine (fig. 10) the amplitudes of the two bands in the wavefunctions of the mixed states, and the phases, i.e., the signs of the square roots, have to be chosen to give the correct limits for $2V << \sqrt{(E_n-E_m)^2-(2V)^2}$, ($2x, 2y \in [0, \pi]$, c.f. ref.29). I' stands for the state of spin I belonging to the three-quasiparticle band. Our measured branching ratio yields V = 47.5 (+1.5, -2.5) keV at spin 45/2. Table 3 gives derived branching ratios which we calculate with this interaction strength, and the experimental values from coincidence spectra. The relative transition rates of all observed or non-observed transitions between the two bands are consistent with the above V.

Changing the order of the 815 keV and 832 keV transitions in the A band would result in a somewhat smaller interaction V≈ 41.5 keV. However, we would then have an inconsistency between the derived and experimental branching ratios, because we do not observe the hypothetical cross-band transition from the $45/2^+$ state of the A band to the ABC band, although the B(E2) ratio should be symmetric for the two $45/2^+$ states.

The interaction strength of the BC crossing compares well with the strength of the AB crossing in ^{166}Yb which is reported to be ≈ 45-50 keV.[11]) Cranked shell-model calculations give an interaction matrix element V for the BC crossing which is some three to four times larger than the value we extract from the data, and suggest that N=95 lies close to the neutron number where the maximum of the interaction is expected (N ≈ 96-97).[20]) The discrepancy in the absolute value of the matrix element is not too unusual if one looks at theoretical and experimental values for the AB crossing.[28]) However, the trend of the interaction strength with neutron number is in general well reproduced in these calculations. Thus, our measurement of the strength of the BC crossing gives some information about the strength in adjacent neutron numbers.

3.3. Alignments in ^{166}Yb

The lower-frequency part of the observed bands in ^{166}Yb was discussed by Walus et al.[11]) In fig. 11 the Routhians of the lowest positive- and negative-parity quasiparticle bands are depicted. The two-quasineutron band AB crosses the ground-state band (vacuum) at $\hbar\omega \approx 0.27$ MeV and stays yrast up to the highest known spins. The (-,1) band is identified as being built on the two-quasiparticle band AE, the BC alignment taking place at the crossing frequency $\hbar\omega \approx 0.31$ MeV. Strong band interaction between these two- and four-quasineutron bands makes this crossing very smooth. (For $N \approx 96$ the maximum of the BC interaction matrix element is expected,[20]) c.f. comments in the previous section.) Its signature partner $(-,0)_1$ is built on the two-quasiparticle state AF. The BC alignment occurs at the same crossing frequency as in the AE band, implying that the E and F orbitals have little signature splitting. This is in agreement with the small signature splitting observed in ^{165}Yb for the EAB and FAB bands (see fig. 8). With increasing frequency the four-quasineutron band ABCE comes closer in energy to the yrast band. This behavior is expected, since the four-quasiparticle band has a larger (relative) alignment i than the two-quasiparticle band ($i = - de'/d\omega$).

Although the continuation of the ground-state band is shown in the Routhian plot of fig. 11, it can be better observed by directly looking at the angular momentum. Fig. 12 shows the continuation of the ground-state band, together with the equivalent states in ^{164}Yb for comparison.[12]) The change in alignment occurs at a frequency $\hbar\omega \approx 0.36$ MeV and amounts in both cases to at least $7\hbar$. The mixing between the ground-state band and the crossing band disturbs the states where the two bands are closest in energy, causing the "wiggles" in the curve. The large gain in alignment is an indication that not only the two-quasineutron orbitals BC are involved, but also AD to form the

four-quasineutron band ABCD, as suggested by Jonsson et al. for the ^{164}Yb case.[12]

The $(-,0)_2$ band has been tentatively interpreted by Jonsson et al. as the band BE[12], being smoothly connected to an octupole band at low rotational frequencies. If so, the AD alignment should be seen in this band. Possibly an alignment starts to develop at the highest observed transitions. Tentatively interpreting this as AD alignment is consistent with the frequency of the observed upbend in the continuation of the ground-state band.

The moment of inertia rises in the yrast band from spin 34^+ to spin 38^+, an indication for alignment (see fig. 14). In the lowest negative-parity band (-,1), an upbend may be starting at the highest spins (see fig. 13). These features may be tentatively ascribed to proton alignment as has already been suggested in two ^{165}Yb bands. The identification of the next few states in all these bands will be necessary to determine this proton crossing unambiguously.

3.4. Constancy of the moments of inertia in ^{166}Yb

The constancy of the moments of inertia at high spin has been observed in a whole series of nuclei, and considerable interest has been associated with it.[1,10,13,30] The spectroscopy of ^{166}Yb reveals one more case where this behavior is found. Fig. 14 shows the kinematic ($\Im^{(1)}=I/\omega$) and dynamic ($\Im^{(2)}=dI/d\omega$) moments of inertia of the yrast band above the AB crossing in ^{166}Yb, together with some other cases where constancy of the moment of inertia was observed.[1,13,30]

All these nuclei have a roughly constant value for $\Im^{(1)}$ and $\Im^{(2)}$ over several transitions. However, lifetime measurements performed in ^{166}Yb using D.S.A.M. techniques show that at these high spins the B(E2) drops by ≈ 40%, probably due to a shape change.[24]) Such an effect would cause a decrease in the collective part of the moment of inertia by 40% if one assumes that the moment of inertia has the same dependence on β and γ as does the B(E2) (e.g., the case for irrotational flow). On the other hand, if the flow pattern of the collective part of the nuclear motion were rigid, the 40% drop in the B(E2) would correspond to a hardly noticeable change in the moment of inertia of the order of a percent. The actual effect on the collective moment of inertia will probably lie between these two limiting cases. Any particle alignment will increase the moment of inertia and will decrease the pairing correlations (due to blocking), as will the Coriolis antipairing, both tending to increase $\Im$. Hence, alignment and pairing loss could compensate the shape change and produce the locally constant effective moment of inertia which we observe in the data. For instance, a gradual alignment of about 9$\hbar$ would be needed to make the moment of inertia look constant in the "worst" case assuming irrotational flow. This amount seems not totally out of the range of alignment which, e.g., a pair of $h_{9/2}$ neutrons or $h_{11/2}$ protons could provide, especially since the value of the collective part of the moment of inertia is not well known and the actually needed alignment is related to it.

Selfconsistent cranking calculations for the ^{168}Hf case[31]) reproduce the constancy of the moment of inertia after the first backbend fairly well and indicate at the same time gradual proton alignment above $I \approx 26^+$ in the yrast band. The smoothness is explained by the large interaction matrix element which one would expect for Z=72.[20]) Calculations of the same type for ^{166}Yb, which has the same neutron number but two protons less, seem to give very similar results.[32]) However, these calculations do not yield a 20% decrease in β over the spin range 26 to 34, but rather a

decrease of the order of a few percent to 10% while γ stays at small negative values (Lund convention). Still, no other explanation has been forthcoming, and so it remains surprising that such an apparently accidental compensation is realized over such a large frequency range in so many nuclei in the well-deformed rare-earth region. It is an interesting problem, whether the shape change is due to the alignment of the same states in all those nuclei, and is thus systematically balanced to result in a constant effective moment of inertia. This whole question remains open today.

4. Conclusions

The two well-deformed nuclei ^{165}Yb and ^{166}Yb produced in the reaction ^{130}Te (^{40}Ar,xn) are studied up to high spins ($77/2^-$ resp. 38^+ in the yrast bands)by means of discrete-line γ spectroscopy. The Berkeley high-energy-resolution array enabled us to register a sufficiently large number of triple or higher-multiple events so that we could analyze double-gated coincidence spectra. The first gate is used to select the product nucleus, the second gate to select a certain band in that nucleus. This method yields particularly clean and simple spectra, and the associated loss in statistics is partially compensated by the possibility to sum many gates in one band. The band structure of the two nuclei studied can be understood on the basis of the cranked-shell model. Both nuclei behave smoothly at high spins beyond the first (neutron) backbend. Only for the very highest transitions an irregularity in the transition energies seems to be present, which is tentatively interpreted as the onset of proton alignment. In ^{165}Yb, we find the continuation of the A band beyond the BC crossing, and evaluate the interaction strength between the two bands employing a

simple four-level model V = 45-49 keV at spin 45/2. In ^{166}Yb, a constant moment of inertia is observed over several high-spin states in the yrast band which is tentatively ascribed to a balance of shape and alignment changes. It would be interesting to find out whether a loss of collectivity is also observed in other nuclei over the spin range where they have a constant moment of inertia and thus the suggested cancellation happens "systematically".

We would like to thank M.K. Lee and R.A. Belshe for help with the electronics and computer software, respectively, and Dr. J.L. Egido for helpful discussions and calculations. One of us (E.M.B.) acknowledges stimulating discussions with Dr. H. Meuth and financial support from the German National Scholarship Foundation. This work was supported by the Director, Office of Energy Research, Division of Nuclear Physics of the Office of High Energy and Nuclear Physics of the U.S. Department of Energy under Contract DE-AC03-76SF00098.

References

1) R. Chapman, J.C. Lisle, J.N. Mo, E. Paul, A. Simcock, J.C. Willmott, J.R. Leslie, H.G. Price, P.M. Walker, J.C. Bacelar, J.D. Garrett, G.B. Hagemann, B. Herskind, A. Holm, P.J. Nolan, Phys. Rev. Lett. 51 (1983) 2265

2) J.C. Bacelar, R. Chapman, J.C. Lisle, J.N. Mo, E. Paul, J.C. Willmott, J.R. Leslie, J.D. Garrett, G.B. Hagemann, B. Herskind, A. Holm, P.M. Walker, Nucl. Phys. A442 (1985) 547

3) F.S. Stephens, M.A. Deleplanque, R.M. Diamond, A.O. Macchiavelli, J.E. Draper, Phys. Rev. Lett. 54 (1985) 2584

4) P.O. Tjøm, R.M. Diamond, J.C. Bacelar, E.M. Beck, M.A. Deleplanque, J.E. Draper, F.S. Stephens, Phys. Rev. Lett. 55 (1985) 2405

5) B. Haas, D. Ward, H.R. Andrews, A.J. Ferguson, J.F. Sharpey-Schafer, T.U. Alexander, W. Trautmann, D. Horn, P. Taras, P. Skensved, T.L. Khoo, R.K. Smither, I. Ahmad, C.N. Davids, W. Kutschera, S.Levenson, C.L. Doors, Nucl. Phys. A362 (1981) 254

6) A. Johnson, H. Ryde and J. Sztarkier, Phys. Lett. 34B (1971) 605

7) F.S. Stephens and R.S. Simon, Nucl. Phys. A183 (1972) 257

8) S.B. Patel, F.S. Stephens, J.C. Bacelar, E.M. Beck, M.A. Deleplanque, R.M. Diamond, J.E. Draper, Phys. Rev. Lett., in press

9) J.C. Bacelar, M. Diebel, O. Andersen, J.D. Garrett, G.B. Hagemann, B. Herskind, J. Kownacki, C.X. Yang, L. Carlen, J. Lyttkens, H. Ryde, W. Walus, P.O. Tjøm, Phys. Lett. 152B (1985) 157

10) C. Schück, N. Bendjaballah, R.M. Diamond, Y. Ellis-Akovali, K.H. Lindenberger, J.O. Newton, F.S. Stephens, J.D. Garrett and B. Herskind, Phys. Lett. 142B (1984) 253

11) W. Walus, N. Roy, S. Jonsson, L. Carlen, H. Ryde, G.B. Hagemann, B. Herskind, J.D. Garrett, Y.S. Chen, J. Almberger, G. Leander, Phys. Scr. 24 (1981) 324

12) S. Jonsson, N. Roy, H. Ryde, W. Walus, J. Kownacki, J.D. Garrett, G.B. Hagemann, B.

Herskind, R. Bengtsson and S. Aberg, Nucl. Phys. A449 (1986) 537

13) J.C. Bacelar, M. Diebel, C. Ellegaard, J.D. Garrett, G.B. Hagemann, B. Herskind, A. Holm, C.X. Yang, J.Y. Zhang, P.O. Tjøm, J.C. Lisle, Nucl. Phys. A442 (1985) 509

14) C. Schück, F. Hannachi, R. Chapman, J.C. Lisle, J.N. Mo, E. Paul, D.J.G. Love, P.J. Nolan, A.H. Nelson, P.M. Walker, Y. Ellis-Akovali, N.R. Johnson, N. Bendjaballah, R.M. Diamond, M.A. Deleplanque, F.S. Stephens, E. Dines, J. Draper, in Proc. XXIII Winter Meeting on nuclear physics, Bormio, Italy, January 1985, ed. I. Iori (Ricerca Scientifica ed Educazione Permanente, Milan, 1985) p. 294

15) R.M. Diamond and F.S. Stephens, The High Resolution Ball, Sept. 1981, unpublished

17) J.E. Draper, E.L. Dines, M.A. Deleplanque, R.M. Diamond, F.S. Stephens, Phys. Rev. Lett. 56 (1986) 309

18) F.S. Stephens, J.E. Draper, J.L. Egido, J.C. Bacelar, E.M. Beck, M.A. Deleplanque, R.M. Diamond, Phys. Rev. Lett., submitted

19) J.E. Draper, Nucl. Instr. and Meth., in press

20) R. Bengtsson and S. Frauendorf, Nucl. Phys. A327 (1979) 139

21) S. Frauendorf, in Proc. Int. Workshop on nuclear physics, ICTP, Trieste 1981, ed. C.H. Dasso et al. (North-Holland, Amsterdam,1982) p.111

22) J.D. Garrett, G.B. Hagemann, B. Herskind, J.C. Bacelar, R. Chapman, J.C. Lisle, J.N. Mo, A. Simcock, J.C. Willmott, H.G. Price, Phys. Lett. 118B (1982) 297

23) Y.S. Chen, S. Frauendorf, L.L. Riedinger, Phys. Lett. 171B (1986) 7

24) J.C. Bacelar, A. Holm, R.M. Diamond, E.M. Beck, M.A. Deleplanque, J.E. Draper, B.Herskind, F.S. Stephens, Phys. Rev. Lett., in press

25) N. Roy, S. Jonsson, H. Ryde, W. Walus, J.J. Gaardhøje, J.D. Garrett, G.B. Hagemann and B. Herskind, Nucl. Phys. A382 (1982) 125

26) L.L. Riedinger, O. Andersen, S. Frauendorf, J.D. Garrett, J.J. Gaardhøje, G.B. Hagemann, B. Herskind, Y.V. Makovetzky, J.C. Waddington, M. Guttormsen, P.O.Tjøm, Phys. Rev.

Lett. 44 (1980) 568

27) C. Schück, N. Bendjaballah, R.M. Diamond, Y. Ellis-Akovali, K.H. Lindenberger, J.O. Newton, S. Shih, F.S. Stephens, J.D. Garrett and B. Herskind, in Proc. XX Winter Meeting on nuclear physics, Bormio, Italy, January 1982, ed. I. Iori (Ricerca Scientifica ed Educazione Permanente, Milan, 1982) p. 197

28) R. Bengtsson, S.Frauendorf, Nucl. Phys. A314 (1979) 27

29) A.S. Davydov, Quantum Mechanics (Pergamon Press, Oxford, 1976^2) p.191 f.

30) J. Recht, Y.K. Agarwal, K.P. Blume, M. Guttormsen, H. Hübel, H. Kluge, K.H. Maier, A. Maj, N. Roy, D.J. Decman, J. Dudek and W. Nazarewicz, Nucl. Phys. A440 (1985) 366

31) U. Mutz and P. Ring, J. of Phys. G: Nucl. Phys. 10 (1984) L39

32) J.L. Egido, June 1986, private communication

Figure captions

Fig. 1. Reaction $^{130}Te(^{40}Ar,4n\text{-}6n)\ ^{166\text{-}164}Yb$. Full projections of the two-dimensional γ-coincidence spectra which were mainly used for the data analyses: a) from full maxtrix, b) from gated matrix in coincidence with discrete lines in ^{165}Yb, c) from gated matrix in coincidence with discrete lines in ^{166}Yb. The strongest lines in ^{165}Yb are marked by open circles, those in ^{166}Yb by full circles and those in ^{164}Yb by crosses.

Fig. 2. One-dimensional background-subtracted spectra in coincidence with the 490 keV transition. a) projection from the full matrix. The gate is contaminated by a transition of the same energy in ^{164}Yb.[10]) The strongest lines in ^{164}Yb are denoted by crosses. b) Projection from gated matrix in coincidence with discrete lines in ^{165}Yb. Only the main transitions in ^{165}Yb in coincidence with the gate are labeled, the numbers indicating the spin of the initial state, c.b. standing for cross-band transition.

Fig. 3. Typical background-subtracted γ-ray spectra which were used for the analysis of ^{165}Yb. Each is the sum of several gated spectra, gates are denoted by "g". a) b) d) Spectra obtained from ^{165}Yb gated matrix. c) Spectrum taken from the full matrix. The given numbers indicate the initial spin of the state from which the γ rays were emitted, c.b. stands for cross-band transition.

Fig. 4. Background-subtracted spectrum showing the ground-state band in ^{166}Yb, projections from the full matrix of the backed-data set. For comments on labeling see fig. 3.

Fig. 5. Typical background-subtracted γ-ray spectra which were used for the construction of the

level scheme of ^{166}Yb. a) Projections from ^{166}Yb gated matrix. b) c) Projections from the full matrix. See fig. 3 for comments on labeling.

Fig. 6. Level scheme of ^{165}Yb as obtained from the present analysis. Cross-band transitions in the lower part of the scheme are partially taken from ref. 10.

Fig. 7. Level scheme of ^{166}Yb as obtained from the present analysis. Cross-band transitions in the lower part of the scheme and the positive-parity band with its band-head at 932 keV are taken from ref. 11.

Fig. 8. Routhians versus $\hbar\omega$ of bands in ^{165}Yb. The rigid-rotor (ß=0.24) reference $\Im=73\,\hbar^2\mathrm{MeV}^{-1}$ was used. Full squares represent the A band, open squares the ABC band, full circles the B band, open circles the E (EAB after the first backbend) and full triangles the FAB band. For all bands K=5/2 was assumed in the transformation to the rotating frame.

Fig. 9. Angular momentum I (taken to be $(I_1+I_2)/2 + 1/2$) plotted versus $\hbar\omega$ for different bands in ^{165}Yb. All bands are represented by the same symbols as in fig. 8.

Fig. 10. Schematic band crossing in a simple four-level model. The dotted lines indicate where the "unperturbed" levels are situated.

Fig. 11. Routhians versus $\hbar\omega$ of bands in ^{166}Yb relative to a rigid-rotor (ß=0.25) reference $\Im=74\hbar^2\mathrm{MeV}^{-1}$. Full circles mark the ground-state band, open circles the AB band, open squares the AE band, full squares the AF band and open triangles the BE band. For the BE band K=5 was assumed in the transformation to the rotating frame, for all other bands

K=0.

Fig. 12. Angular momentum I versus $\hbar\omega$ for the ground-state band of ^{166}Yb (full circles) and ^{164}Yb (open circles). The data for ^{164}Yb are taken from ref.12.

Fig.13. Angular momentum I versus $\hbar\omega$ for bands in ^{166}Yb. All bands are represented by the same symbols as in fig. 11.

Fig.14. a) - d) Kinematic $\mathfrak{I}^{(1)}$ (full squares) and dynamic $\mathfrak{I}^{(2)}$ (open squares) moments of inertia in units of $\hbar^2$MeV^{-1} plotted versus $\hbar\omega$. For comparison the yrast bands of several well-deformed rare-earth nuclei with remarkably constant moment of inertia are shown. The data for ^{168}Yb, ^{168}Hf and ^{170}W are taken from refs. 13, 1 and 30.

Table 1: Summary of experimental results on ^{165}Yb

E_γ(keV)[a]	I_γ[b]	I_{900}/I_{400}[c]	Assignment
197.4	12.8	1.06 (9)	(-,+1/2) $9/2^- \rightarrow 5/2^-$
202.5	10.1 f)	1.4 (2)	cross band $15/2^+ \rightarrow 13/2^+$
205.8	84	1.13 (6)	$(+,+1/2)_1$ $17/2^+ \rightarrow 13/2^+$
209.6	20	0.84 (12)	(+,-1/2) $15/2^+ \rightarrow 11/2^+$
275.0	2.2	e)	cross band $13/2^- \rightarrow 11/2^+$
287.0	20	1.14 (10)	(-,+1/2) $13/2^- \rightarrow 9/2^-$
322.2	100	1.00	$(+,+1/2)_1$ $21/2^+ \rightarrow 17/2^+$
335.3	6.4	1.9 (5) f)	cross band $19/2^+ \rightarrow 17/2^+$
338	e)	e)	cross band $33/2^- \rightarrow 31/2^+$
339.0	d)	0.83 (10)	(+,-1/2) $19/2^+ \rightarrow 15/2^+$
365.7	19.4	1.09 (10)	(-,+1/2) $17/2^- \rightarrow 13/2^-$
429.2	92	0.97 (5)	$(+,+1/2)_1$ $25/2^+ \rightarrow 21/2^+$
430.6	d)	1.15 (10)	(-,+1/2) $21/2^- \rightarrow 17/2^-$
431	d)	d)	cross band $17/2^- \rightarrow 15/2^+$
453.2	23	0.83 (8)	(+,-1/2) $23/2^+ \rightarrow 19/2^+$
465.7	4.4	1.3 (3)	cross band $23/2^+ \rightarrow 21/2^+$
469.3	4.0	0.89 (18)	(-,-1/2) $31/2^- \rightarrow 27/2^-$

477.6			(-,+1/2) $25/2^- \rightarrow 21/2^-$
	56	0.99 (8)	
477.6			(-,+1/2) $33/2^- \rightarrow 29/2^-$
488.5	d)	d)	cross band $29/2^- \rightarrow 27/2^+$
490.2	29	1.11 (9)	(-,+1/2) $29/2^- \rightarrow 25/2^-$
505.9	10.7	1.01 (14)	(-,-1/2) $35/2^- \rightarrow 31/2^-$
516.7	28	0.97 (8)	(-,+1/2) $37/2^- \rightarrow 33/2^-$
522.7	3.4	2.0 (6)	cross band $21/2^- \rightarrow 19/2^+$
523.6	79	0.90 (5)	$(+,+1/2)_1$ $29/2^+ \rightarrow 25/2^+$
533	d)	d)	$(+,+1/2)_2$ $41/2^+ \rightarrow 37/2^+$
542.0	4.1 f)	e)	cross band $39/2^- \rightarrow 37/2^+$
547.2	1.9	2.1 (5)	cross band $25/2^- \rightarrow 23/2^+$
549.3	23	0.94 (13)	(+,-1/2) $27/2^+ \rightarrow 23/2^+$
566.1	17.8	0.70 (10)	(-,-1/2) $39/2^- \rightarrow 35/2^-$
577	1.0	1.0 (3)	$(+,+1/2)_2$ $45/2^+ \rightarrow 41/2^+$
580.8	25	1.03 (12)	(-,+1/2) $41/2^- \rightarrow 37/2^-$
586.8	6.1	1.6 (2)	cross band $27/2^+ \rightarrow 25/2^+$
605.5	66	0.97 (5)	$(+,+1/2)_1$ $33/2^+ \rightarrow 29/2^+$
629.3	10.6	0.93 (13)	(+,-1/2) $31/2^+ \rightarrow 27/2^+$
635.3	14.1	0.75 (11)	(-,-1/2) $43/2^- \rightarrow 39/2^-$
648.9	21	0.97 (11)	(-,+1/2) $45/2^- \rightarrow 41/2^-$

650.5	10.7	1.5 (2)	cross band $35/2^- \rightarrow 33/2^+$
675.0	45	1.00 (8)	$(+,+1/2)_1$ $37/2^+ \rightarrow 33/2^+$
680	4.1	0.78 (11)	cross band $45/2^+ \rightarrow 41/2^+$
695.2	6.3	0.63 (19)	$(+,-1/2)$ $35/2^+ \rightarrow 31/2^+$
705.7	10.0	1.03 (13)	$(-,-1/2)$ $47/2^- \rightarrow 43/2^-$
715.7	16.2	0.81 (10)	$(-,+1/2)$ $49/2^- \rightarrow 45/2^-$
728.4	41	0.90 (7)	$(+,+1/2)_1$ $41/2^+ \rightarrow 37/2^+$
728.4			cross band $45/2^+ \rightarrow 41/2^+$
734.9	11.0	0.95 (12)	$(+,+1/2)_2$ $49/2^+ \rightarrow 45/2^+$
749.4	3.9	0.7 (2)	$(+,-1/2)$ $39/2^+ \rightarrow 35/2^+$
750.4	9.9	1.5 (3)	cross band $31/2^- \rightarrow 29/2^+$
773.2	8.2	0.88 (12)	$(-,-1/2)$ $51/2^- \rightarrow 47/2^-$
781.8	10.6	0.77 (11)	$(-,+1/2)$ $53/2^- \rightarrow 49/2^-$
788.0	1.7	e)	$(+,-1/2)$ $43/2^+ \rightarrow 39/2^+$
804.2	4.9 f)	1.7 (5)	cross band $27/2^- \rightarrow 25/2^+$
815.1	7.5	1.11 (15)	$(+,+1/2)_2$ $53/2^+ \rightarrow 49/2^+$
815.4	5.5	1.4 (4)	$(+,+1/2)_1$ $49/2^+ \rightarrow 45/2^+$
831.6	7.0	0.84 (17)	$(+,+1/2)_1$ $45/2^+ \rightarrow 41/2^+$
838.7	5.0	1.23 (17)	$(-,-1/2)$ $55/2^- \rightarrow 51/2^-$

847.0	7.7	1.03 (18)	(-,+1/2) $57/2^- \rightarrow 53/2^-$
851	< 1	e)	(+,-1/2) $47/2^+ \rightarrow 43/2^+$
864.3	3.6	0.9 (3)	$(+,+1/2)_1$ $53/2^+ \rightarrow 49/2^+$
880	3.1	e)	cross band $41/2^+ \rightarrow 37/2^+$
895.3	4.6	0.77 (14)	$(+,+1/2)_2$ $57/2^+ \rightarrow 53/2^+$
901.0	1.6	0.77 (19)	$(+,+1/2)_1$ $57/2^+ \rightarrow 53/2^+$
904.0	4.0	1.1 (2)	(-,-1/2) $59/2^- \rightarrow 55/2^-$
912.4	4.5	0.82 (18)	(-,+1/2) $61/2^- \rightarrow 57/2^-$
937	1.0	0.8 (3)	$(+,+1/2)_1$ $61/2^+ \rightarrow 57/2^+$
964.6	3.8	0.77 (17)	$(+,+1/2)_2$ $61/2^+ \rightarrow 57/2^+$
966.6	2.0	0.9 (3)	(-,-1/2) $63/2^- \rightarrow 59/2^-$
974.8	2.8	1.0 (3)	(-,+1/2) $65/2^- \rightarrow 61/2^-$
1020.4	1.8	0.8 (3)	$(+,+1/2)_2$ $65/2^+ \rightarrow 61/2^+$
1022	2.0	e)	cross band $37/2^+ \rightarrow 33/2^+$
1024.4	1.4	1.0 (3)	(-,-1/2) $67/2^- \rightarrow 63/2^-$
1029.9	2.2	1.0 (3)	(-,+1/2) $69/2^- \rightarrow 65/2^-$
1053	< 1	e)	(-,+1/2) $77/2^- \rightarrow 73/2^-$
1058	1.3	e)	$(+,+1/2)_2$ $69/2^+ \rightarrow 65/2^+$
1060.1	0.7	1.2 (4)	(-,+1/2) $73/2^- \rightarrow 69/2^-$

a) γ-ray energies obtained from gated coincidence spectra. The energies of transitions in the lower part of the level scheme are partly taken from previous studies. Uncertainties in energies are 0.2 keV apart from weakest transitions, where they may be 0.5 keV.

b) γ-ray intensities are mostly obtained from gated coincidence spectra and normalized to the 322.2 keV $21/2^+ \rightarrow 17/2^+$ transition. Intensity values are known to 10 % apart from weakest peaks for which uncertainties can be up to 50 %.

c) Ratios are obtained from coincidence spectra (gated on E2-transitions as described in section 2.3.) and normalized to the 322.2 keV $21/2^+ \rightarrow 17/2^+$ E2-transition. E2-transitions above spin ≈ $29/2^+$ have values systematically below one due to deorientation of the reference state.

d) Masked by a transition of the same energy in ^{164}Yb, ^{165}Yb or ^{166}Yb.

e) Value cannot be obtained because of proximity of a stronger transition or weakness of the transition itself.

f) Probably contaminated by another transition.

Table 2: Summary of experimental results on ^{166}Yb

E_γ(keV)[a]	I_γ[b]	$I_{90°}/I_{40°}$[c]	Assignment
113	0.5	e)	cross band $8^-\rightarrow7^-$
152	0.8	e)	cross band $10^-\rightarrow9^-$
206	5.0	1.04 (13)	$(-,0)_1$ $8^-\rightarrow6^-$
227.9	100	1.00	$(+,0)_1$ $4^+\rightarrow2^+$
248	0.5	e)	$(-,0)_1$ $6^-\rightarrow(4^-)$
289.2	6.5	1.07 (12)	$(-,0)_1$ $10^-\rightarrow8^-$
289	d)	d)	cross band $4^-\rightarrow 5^+$
301.2	2.1	0.9 (3)	$(-,0)_2$ $8^-\rightarrow6^-$
337.5	93	0.97 (5)	$(+,0)_1$ $6^+\rightarrow4^+$
354.4	2.1	0.7 (2)	$(-,0)_2$ $10^-\rightarrow8^-$
356	1.1	e)	cross band $12^+\rightarrow12^+$
366	1.4	1.0 (2)	$(+,0)_2$ $14^+\rightarrow12^+$
367.0	11	1.03 (12)	$(-,0)_1$ $12^-\rightarrow10^-$
375.8	7.0	1.00 (12)	$(+,0)_2$ $16^+\rightarrow14^+$
400.0	3.0	1.1 (3)	$(-,0)_2$ $12^-\rightarrow10^-$
430.2	90	0.88 (6)	$(+,0)_1$ $8^+\rightarrow6^+$

437.6	12	0.98 (12)	$(-,0)_1$ $14^- \rightarrow 12^-$
445.9	3.0	0.90 (18)	$(-,1)$ $13^- \rightarrow 11^-$
459.0	3.0	0.66 (17)	$(-,0)_2$ $14^- \rightarrow 12^-$
490.8	10.0	0.92 (9)	$(-,1)$ $15^- \rightarrow 13^-$
494.3	31	0.77 (4)	cross band $16^+ \rightarrow 14^+$
499.4	13.2	0.96 (10)	$(-,0)_1$ $16^- \rightarrow 14^-$
507.2	123	0.85 (4)	$(+,0)_1$ $10^+ \rightarrow 8^+$
508.3			$(+,0)_2$ $18^+ \rightarrow 16^+$
527.7	2.2	e)	$(-,0)_2$ $16^- \rightarrow 14^-$
538.1	12.0	0.71 (12)	$(-,1)$ $17^- \rightarrow 15^-$
552.8	12	0.71 (12)	$(-,0)_1$ $18^- \rightarrow 16^-$
569.4	64	0.84 (4)	$(+,0)_1$ $12^+ \rightarrow 10^+$
575.1	3.2	1.6 (4)	cross band $15^- \rightarrow 14^+$
586.5	11.1	0.74 (11)	$(-,1)$ $19^- \rightarrow 17^-$
588.5	31	0.74 (5)	$(+,0)_2$ $20^+ \rightarrow 18^+$
592.5	7.1	0.64 (12)	cross band $16^+ \rightarrow 14^+$
592.7	2.0	e)	$(-,0)_2$ $18^- \rightarrow 16^-$
600.4	9.5	0.76 (12)	$(-,0)_1$ $20^- \rightarrow 18^-$

603.6	48	0.89 (12)	$(+,0)_1$ $14^+ \rightarrow 12^+$
630.0	6.5	0.75 (15)	$(-,1)$ $21^- \rightarrow 19^-$
648.3	1.9	d)	$(-,0)_2$ $20^- \rightarrow 18^-$
649.4	8.2	0.87 (12)	$(-,0)_1$ $22^- \rightarrow 20^-$
666.3	22	0.76 (7)	$(+,0)_2$ $22^+ \rightarrow 20^+$
674.0	6.1	0.95 (13)	$(-,1)$ $23^- \rightarrow 21^-$
687.8	6.9	1.4 (4)	cross band $13^- \rightarrow 12^+$
694.9	1.4	e)	$(-,0)_2$ $22^- \rightarrow 20^-$
699.8	7.5	1.01 (12)	$(+,0)_1$ $18^+ \rightarrow 16^+$
704.8	7.5	0.98 (15)	$(-,0)_1$ $24^- \rightarrow 22^-$
710.5	11.3	1.03 (12)	$(+,0)_1$ $16^+ \rightarrow 14^+$
722.1	15.0	1.02 (12)	cross band $14^+ \rightarrow 12^+$
724.9	5.0	0.65 (13)	$(-,1)$ $25^- \rightarrow 23^-$
726.9	4.3	1.0 (2)	$(+,0)_1$ $22^+ \rightarrow 20^+$
728.5	1.9	1.0 (2)	$(+,0)_1$ $24^+ \rightarrow 22^+$
732.9	5.9	1.0 (2)	$(+,0)_1$ $20^+ \rightarrow 18^+$
737.8	1.2	e)	$(-,0)_2$ $24^- \rightarrow 22^-$
738.6	16.2	0.68 (12)	$(+,0)_2$ $24^+ \rightarrow 22^+$
766.6	5.8	0.9 (2)	$(-,0)_1$ $26^- \rightarrow 24^-$

783	1.0	e)	$(-,0)_2$ $26^- \rightarrow 24^-$
787.1	4.6	0.9 (2)	$(-,1)$ $27^- \rightarrow 25^-$
806.3	12.0	0.89 (10)	$(+,0)_2$ $26^+ \rightarrow 24^+$
811.6	5.8 f)	1.33 (19) f)	cross band $11^- \rightarrow 10^+$
833.6	5.1	0.77 (14)	$(-,0)_1$ $28^- \rightarrow 26^-$
853.8	3.5	0.75 (16)	$(-,1)$ $29^- \rightarrow 27^-$
860	0.6	e)	cross band $7^- \rightarrow 8^+$
870.2	7.8	1.00 (13)	$(+,0)_2$ $28^+ \rightarrow 26^+$
903.4	3.1	0.7 (2)	$(-,0)_1$ $30^- \rightarrow 28^-$
922.8	2.5	0.50 (17)	$(-,1)$ $31^- \rightarrow 29^-$
935.0	6.4	0.82 (15)	$(+,0)_2$ $30^+ \rightarrow 28^+$
971.6	1.3	0.7 (2)	$(-,0)_1$ $32^- \rightarrow 30^-$
986.2	1.6	0.7 (2)	$(-,1)$ $33^- \rightarrow 31^-$
998.8	3.7	0.77 (15)	$(+,0)_2$ $32^+ \rightarrow 30^+$
1037	2.5	e)	cross band $7^+ \rightarrow 6^+$
1045	1.3	e)	$(-,1)$ $35^- \rightarrow 33^-$
1053	1.0	e)	cross band $9^+ \rightarrow 8^+$
1060	2.9	1.4 (3) f)	$(+,0)_2$ $34^+ \rightarrow 32^+$
1084	1.0	e)	$(-,1)$ $37^- \rightarrow 35^-$
1111.2	2.5	e)	cross band $9^- \rightarrow 8^+$

1112	1.6	1.0 (3)	$(+,0)_2$ $36^+ \rightarrow 34^+$
1122	0.8	e)	cross band $5^- \rightarrow 6^+$
1158	1.0	e)	$(+,0)_2$ $38^+ \rightarrow 36^+$
1290	1.2	e)	cross band $7^- \rightarrow 6^+$

a) d) e) f) See table 1.

b) γ-ray intensities are mostly obtained from gated coincidence spectra and normalized to the 227.9 keV $4^+ \rightarrow 2^+$ transition. Intensity values are known to 10 % apart from weakest peaks for which uncertainties can be up to 50 %.

c) Ratios are obtained from coincidence spectra (gated on E2-transitions as described in section 2.3.) and normalized to the 227.9 keV $4^+ \rightarrow 2^+$ transition. E2-transitions above spin $\approx 10^+$ have ratios systematically below one due to deorientation of the reference state.

Table 3: Experimental and derived branching ratios involving the A and ABC bands in ^{165}Yb

B(E2) ratio [a]	Experiment		Calculation
$\frac{B(E2;45/2^+_2 \rightarrow 41/2^+_1)}{B(E2;45/2^+_2 \rightarrow 41/2^+_2)}$	$\frac{+0.3}{1.5}$ $\frac{}{-0.3}$	$\rightarrow$	$\frac{+1.5}{V(keV) = 47.5}$ $\frac{}{-2.5}$
$\frac{B(E2;45/2^+_1 \rightarrow 41/2^+_2)}{B(E2;45/2^+_1 \rightarrow 41/2^+_1)}$	$\frac{+0.5}{1.4}$ $\frac{}{-0.5}$		$\frac{+0.3}{1.5}$ $\frac{}{-0.3}$
$\frac{B(E2;49/2^+_2 \rightarrow 45/2^+_1)}{B(E2;49/2^+_2 \rightarrow 45/2^+_2)}$	$\frac{}{< 0.21}$ $\frac{}{}$		$\frac{+0.02}{0.081}$ $\frac{}{-0.02}$
$\frac{B(E2;41/2^+_2 \rightarrow 37/2^+_1)}{B(E2;41/2^+_2 \rightarrow 37/2^+_2)}$	$\frac{+0.08}{0.08}$ $\frac{}{-0.04}$		$\frac{+0.003}{0.038}$ $\frac{}{-0.005}$

a) The subscript n at each spin indicates to which configuration $(+,1/2)_n$ the state belongs.

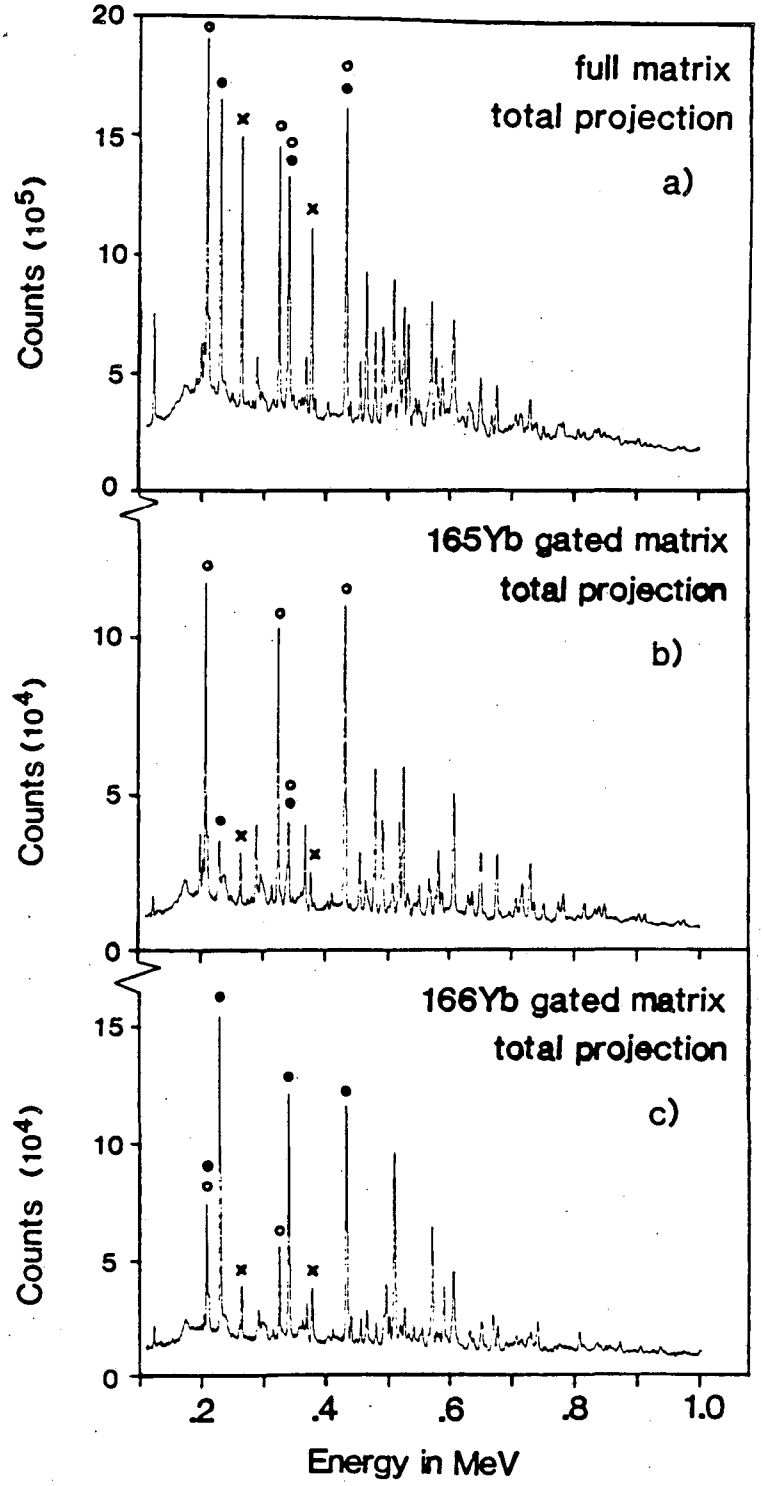
full matrix
total projection
a)
Counts (10^5)
165Yb gated matrix
total projection
b)
Counts (10^4)
166Yb gated matrix
total projection
c)
Counts (10^4)
Energy in MeV
XBL 865-2090

Fig. 1

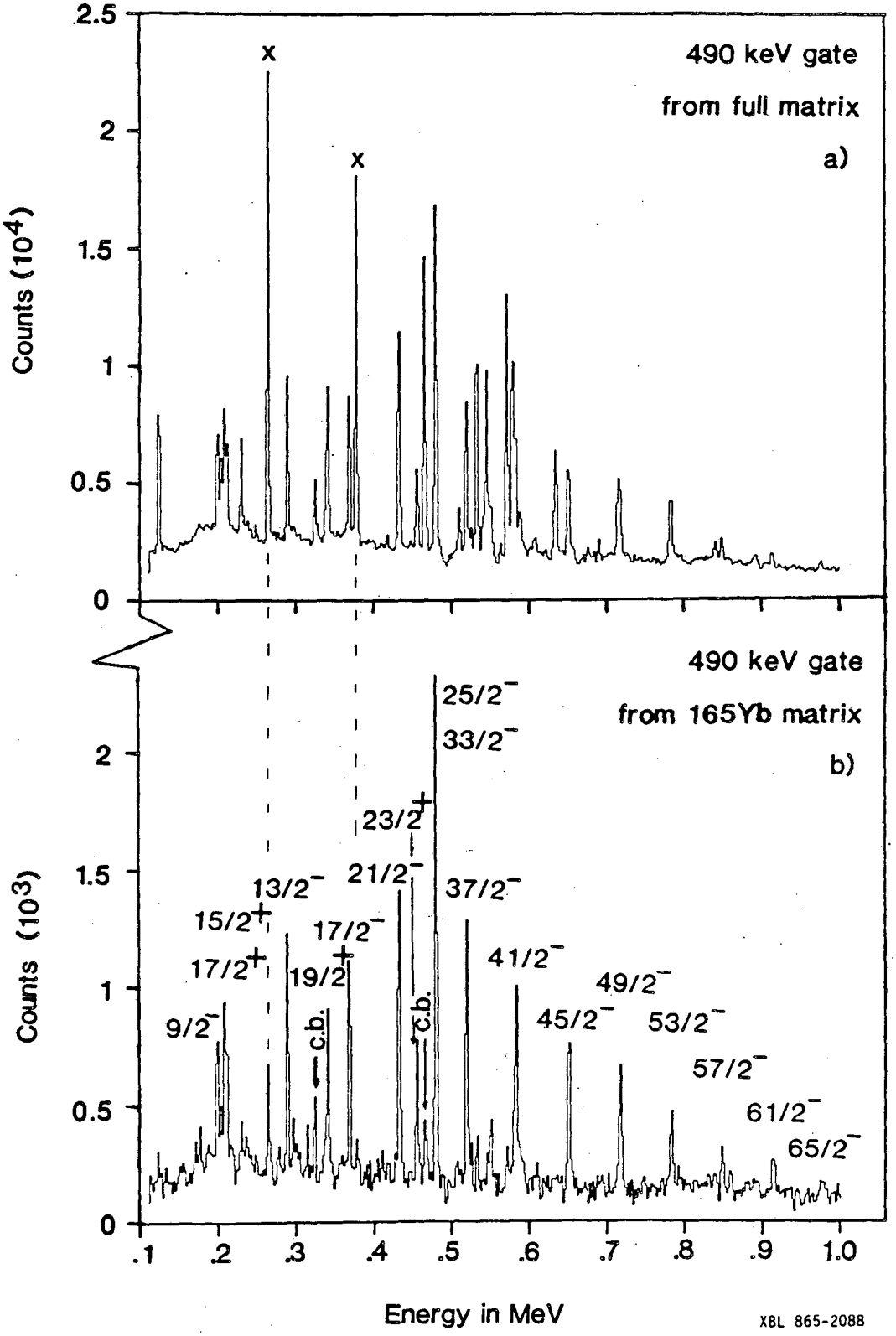
490 keV gate
from full matrix
a)
x
x
Counts (10^4)
2.5
2
1.5
1
0.5
0
490 keV gate
from 165Yb matrix
b)
25/2⁻
33/2⁻
23/2⁺
21/2⁻
37/2⁻
13/2⁻
15/2⁺
17/2⁻
17/2⁺
19/2⁺
41/2⁻
49/2⁻
45/2⁻
53/2⁻
57/2⁻
61/2⁻
65/2⁻
9/2⁻
c.b.
c.b.
Counts (10^3)
2
1.5
1
0.5
0
.1
.2
.3
.4
.5
.6
.7
.8
.9
1.0
Energy in MeV
XBL 865-2088

Fig. 2

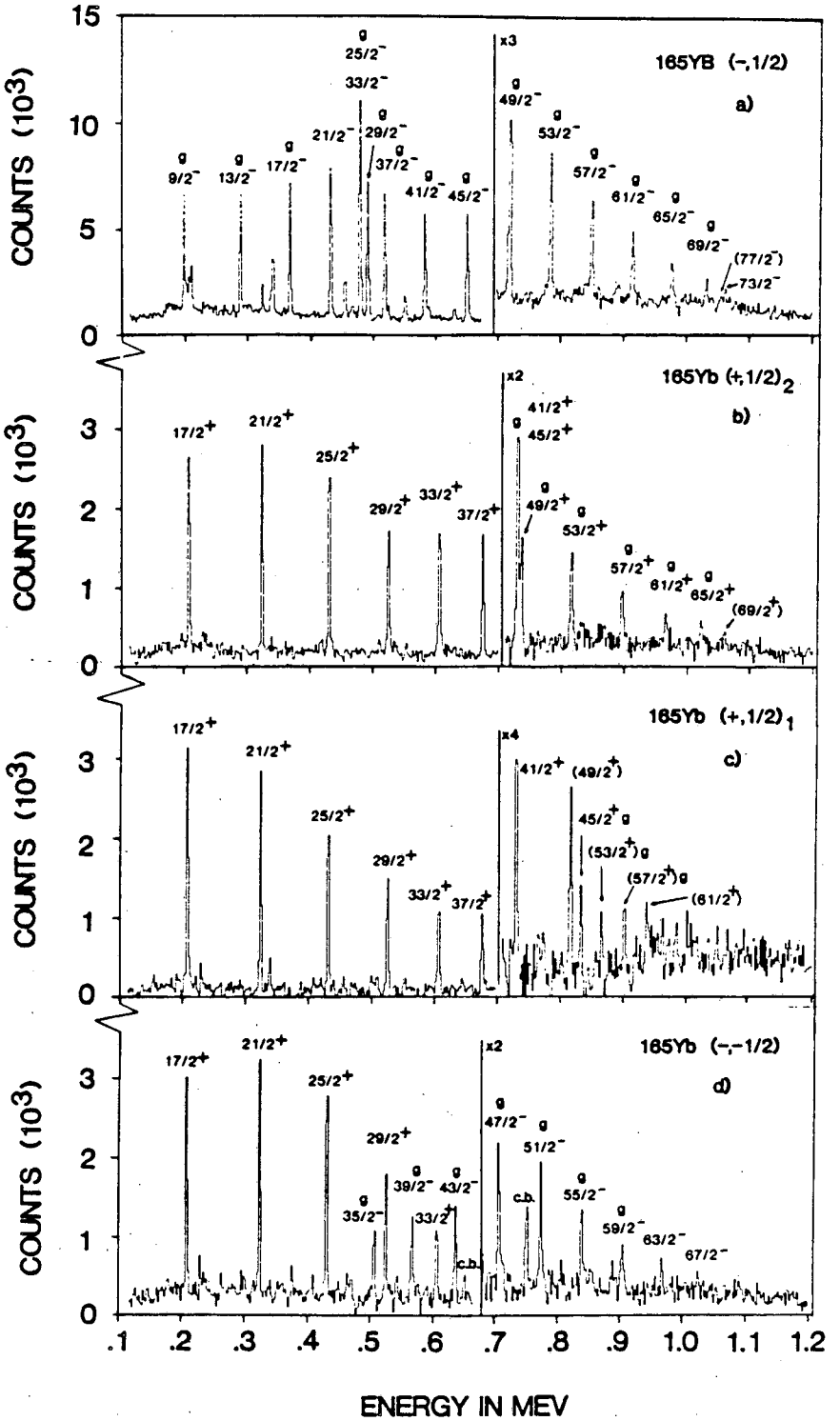
165YB (-,1/2)
a)
165Yb (+,1/2)2
b)
165Yb (+,1/2)1
c)
165Yb (-,-1/2)
d)
COUNTS (10^3)
ENERGY IN MEV
XBL 865-2097

Fig. 3

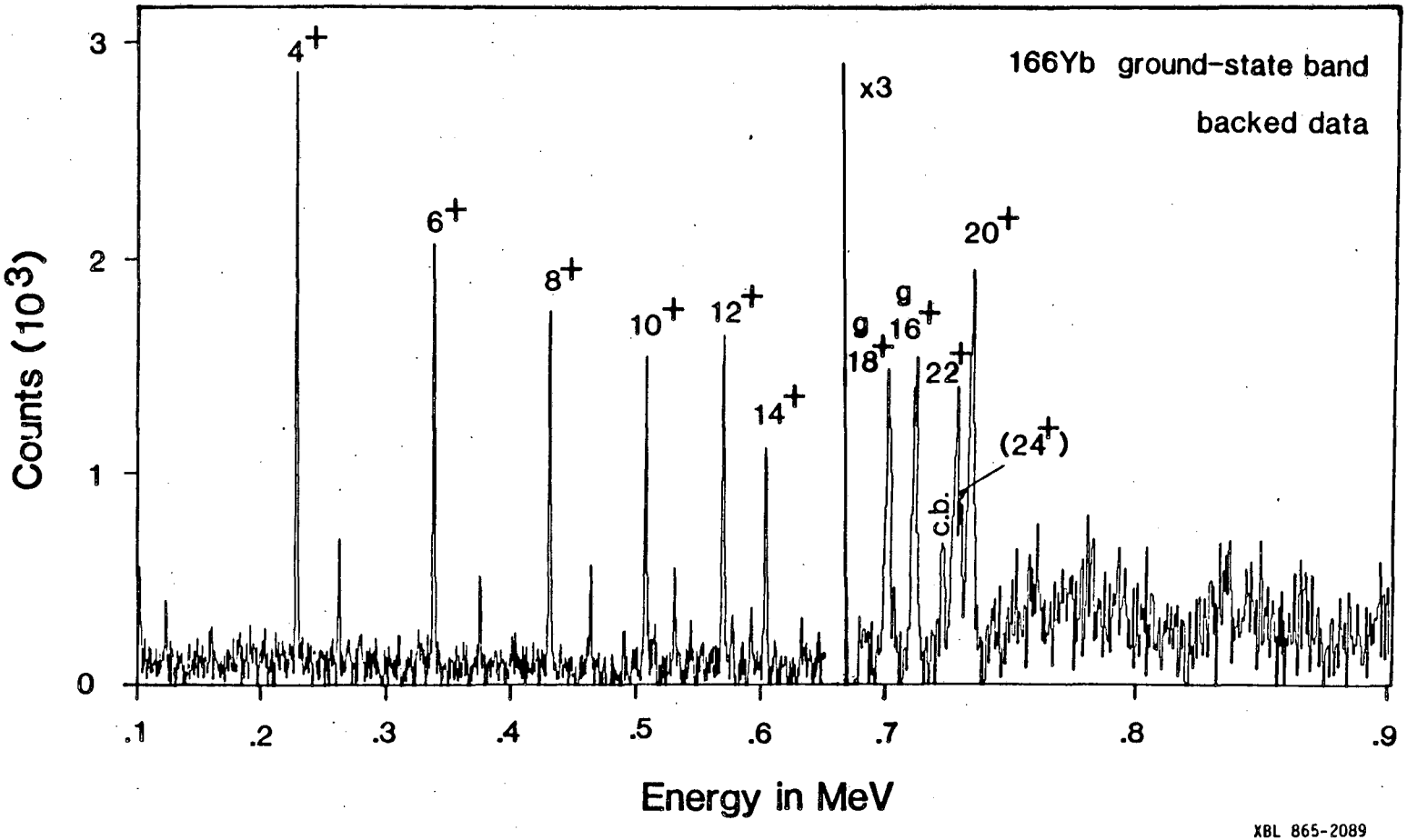
166Yb ground-state band
backed data
x3
4+
6+
8+
10+
12+
14+
16+
18+
20+
22+
(24+)
g
g
c.g.
Counts (10^3)
Energy in MeV
0
1
2
3
.1
.2
.3
.4
.5
.6
.7
.8
.9
XBL 865-2089

Fig. 4

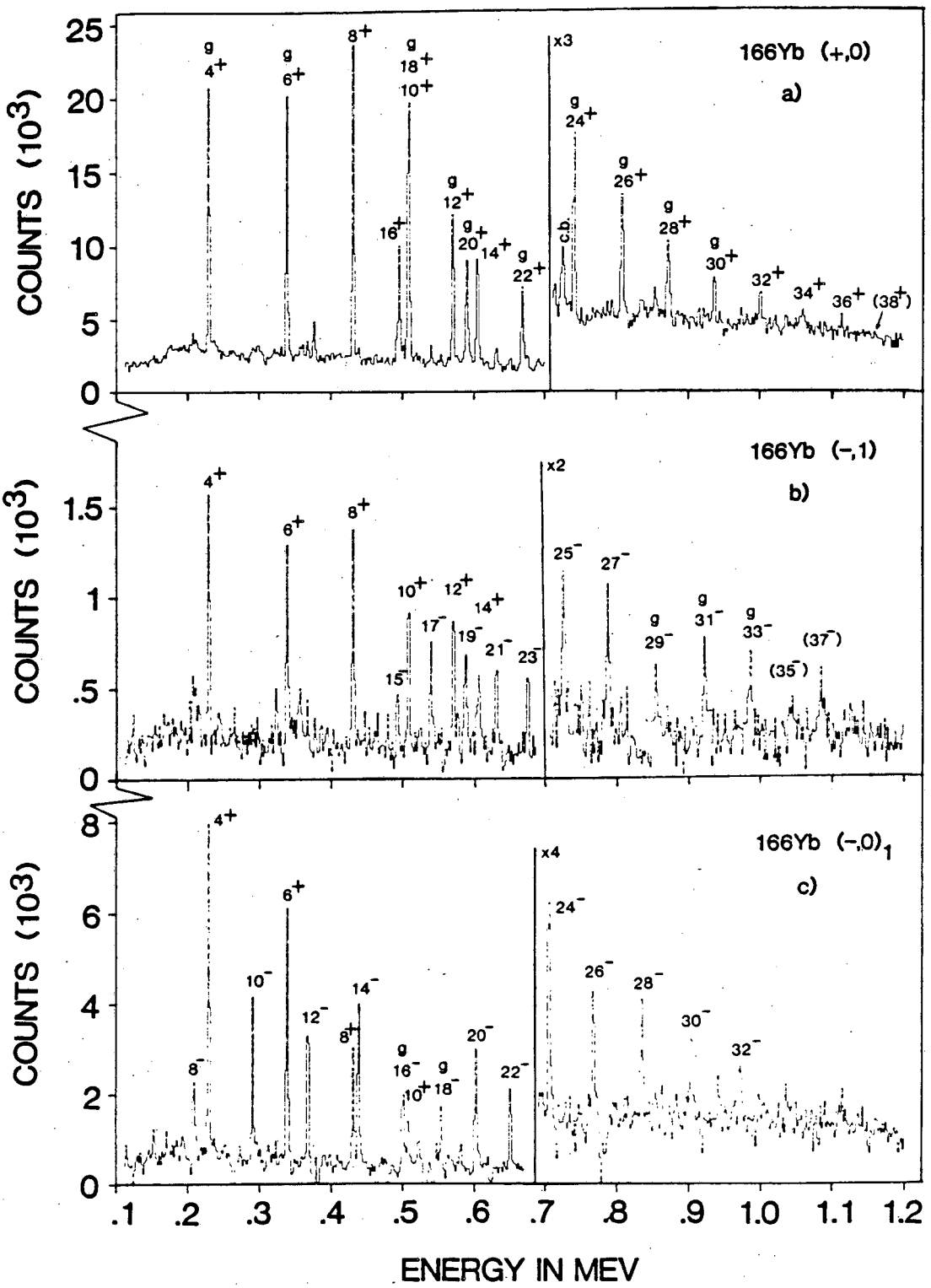
166Yb (+,0)
a)
166Yb (−,1)
b)
166Yb (−,0)1
c)
COUNTS (10^3)
ENERGY IN MEV
XBL 865-2101

Fig. 5

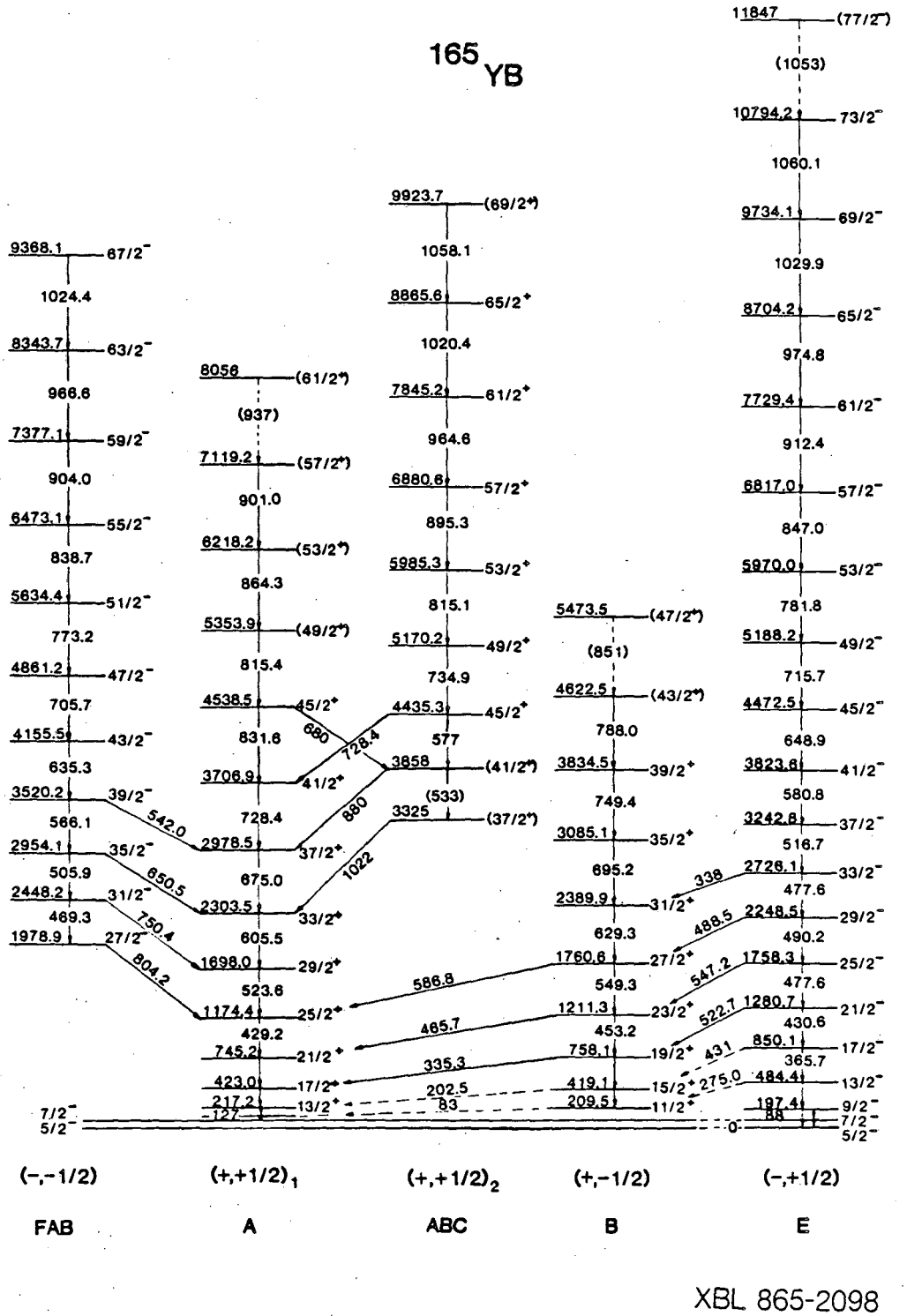

XBL 865-2098

Fig. 6

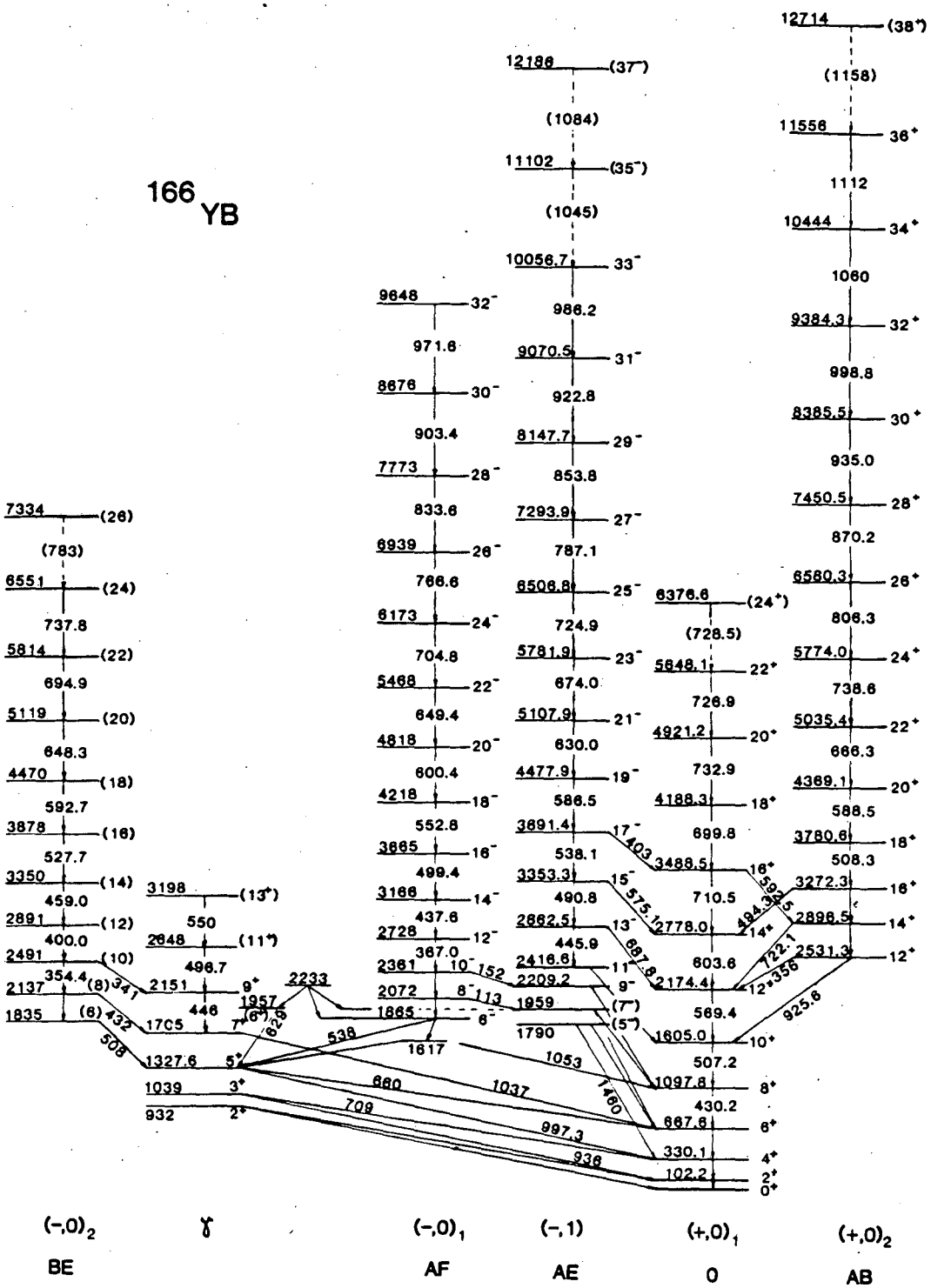

XBL 865-2099

Fig. 7

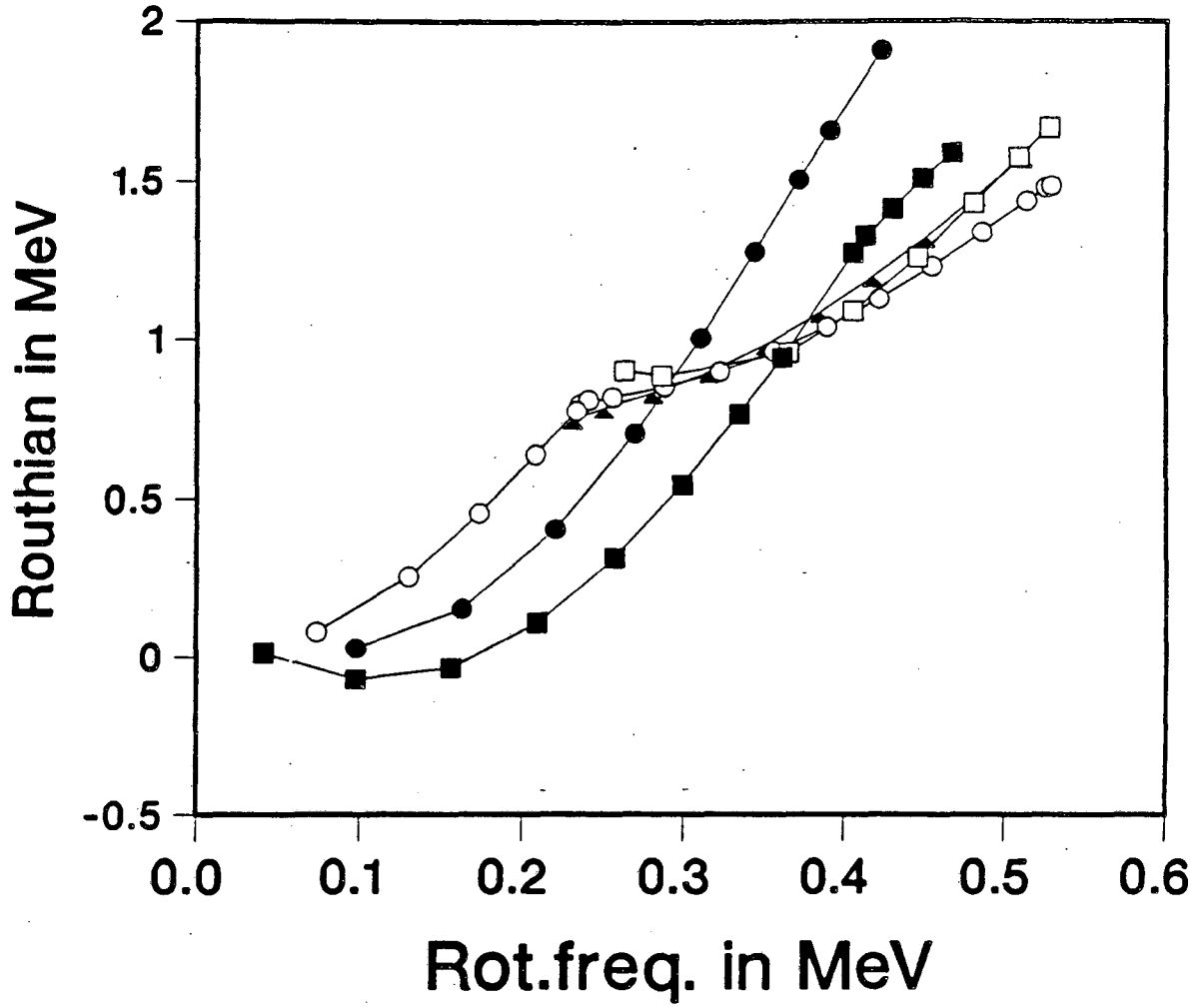

XBL 865-2094

Fig. 8

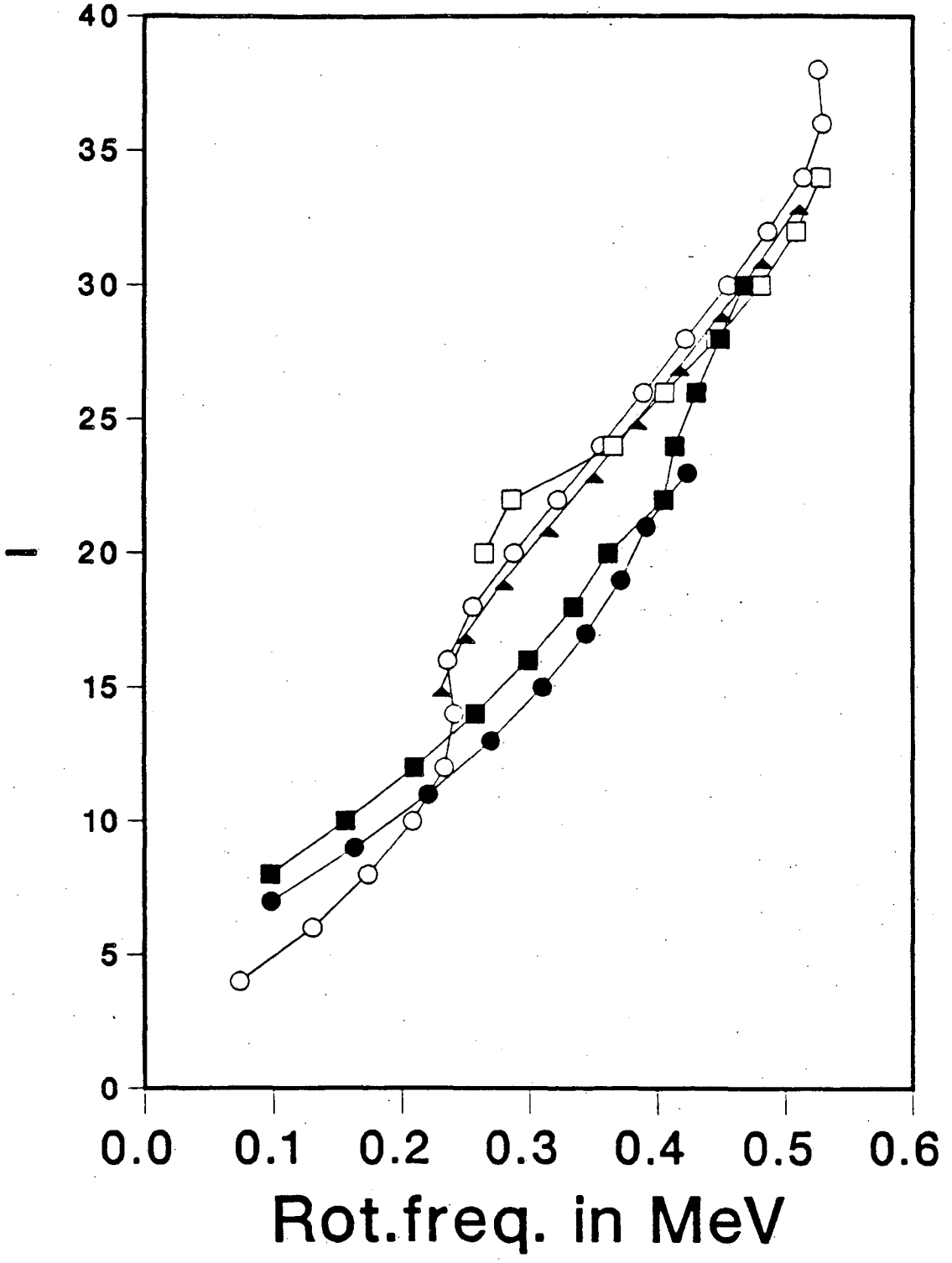

XBL 865-2096A

Fig. 9

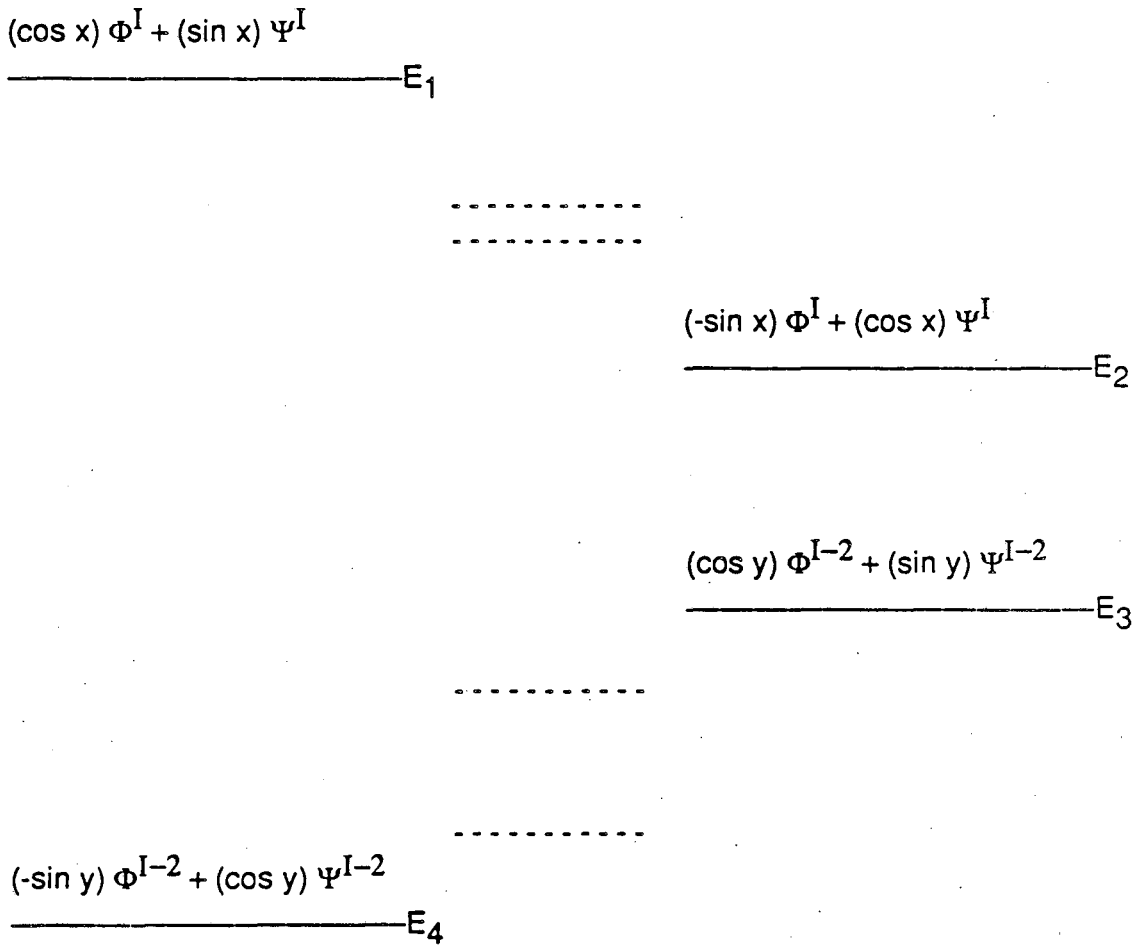

XBL 865-2095

Fig. 10

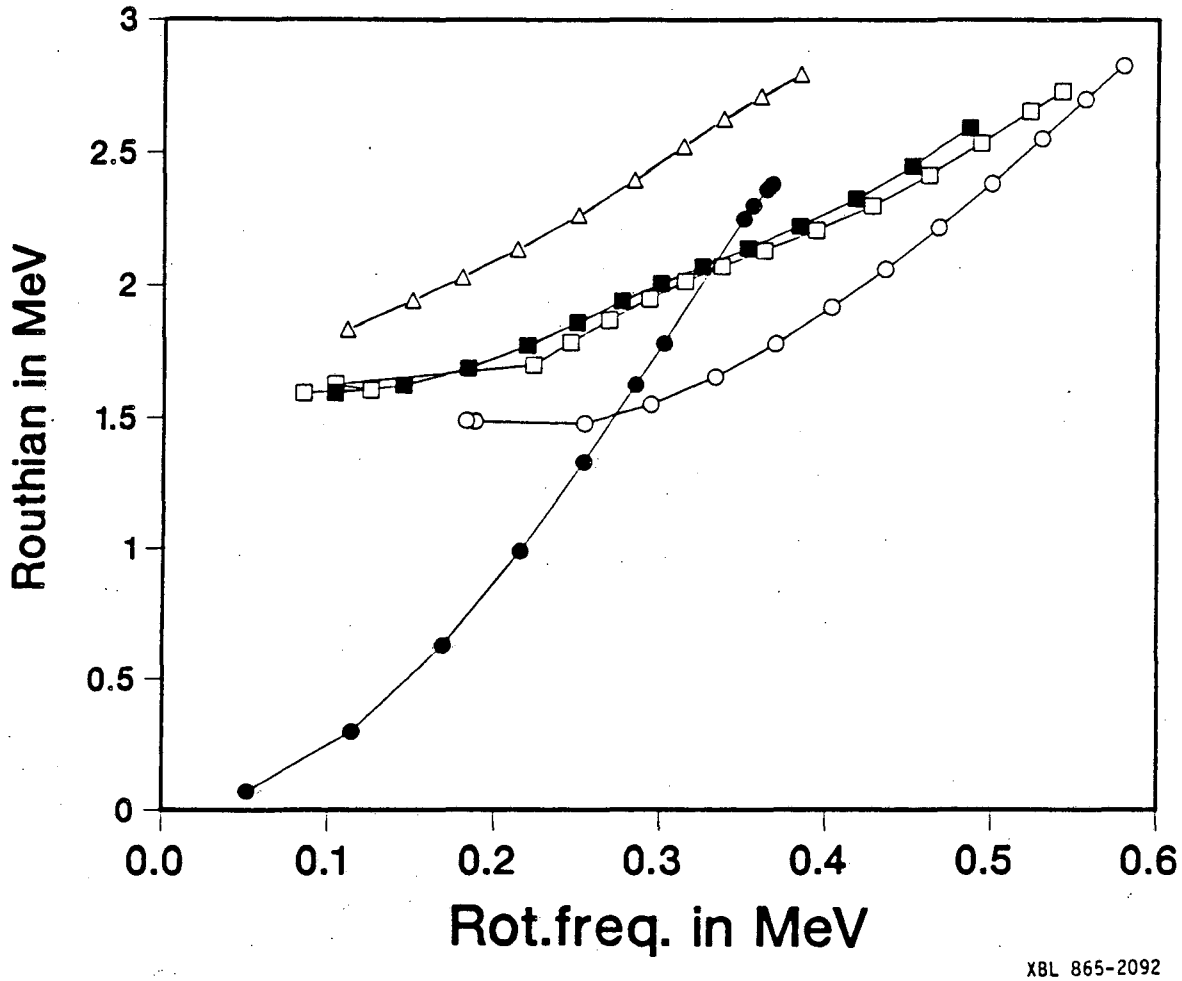
Routhian in MeV
Rot.freq. in MeV
0
0.5
1
1.5
2
2.5
3
0.0
0.1
0.2
0.3
0.4
0.5
0.6
XBL 865-2092

Fig. 11

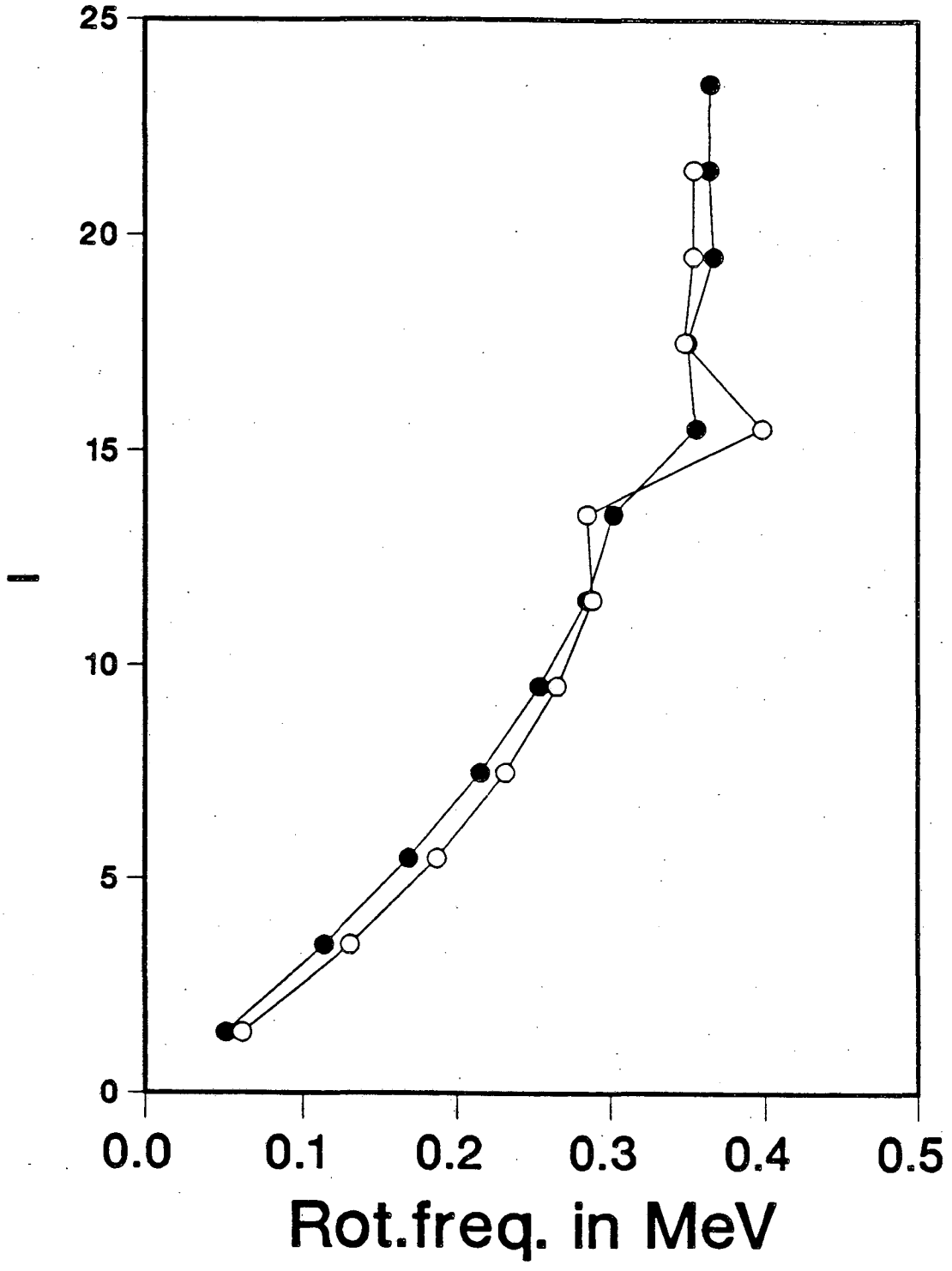

XBL 865-2093

Fig. 12

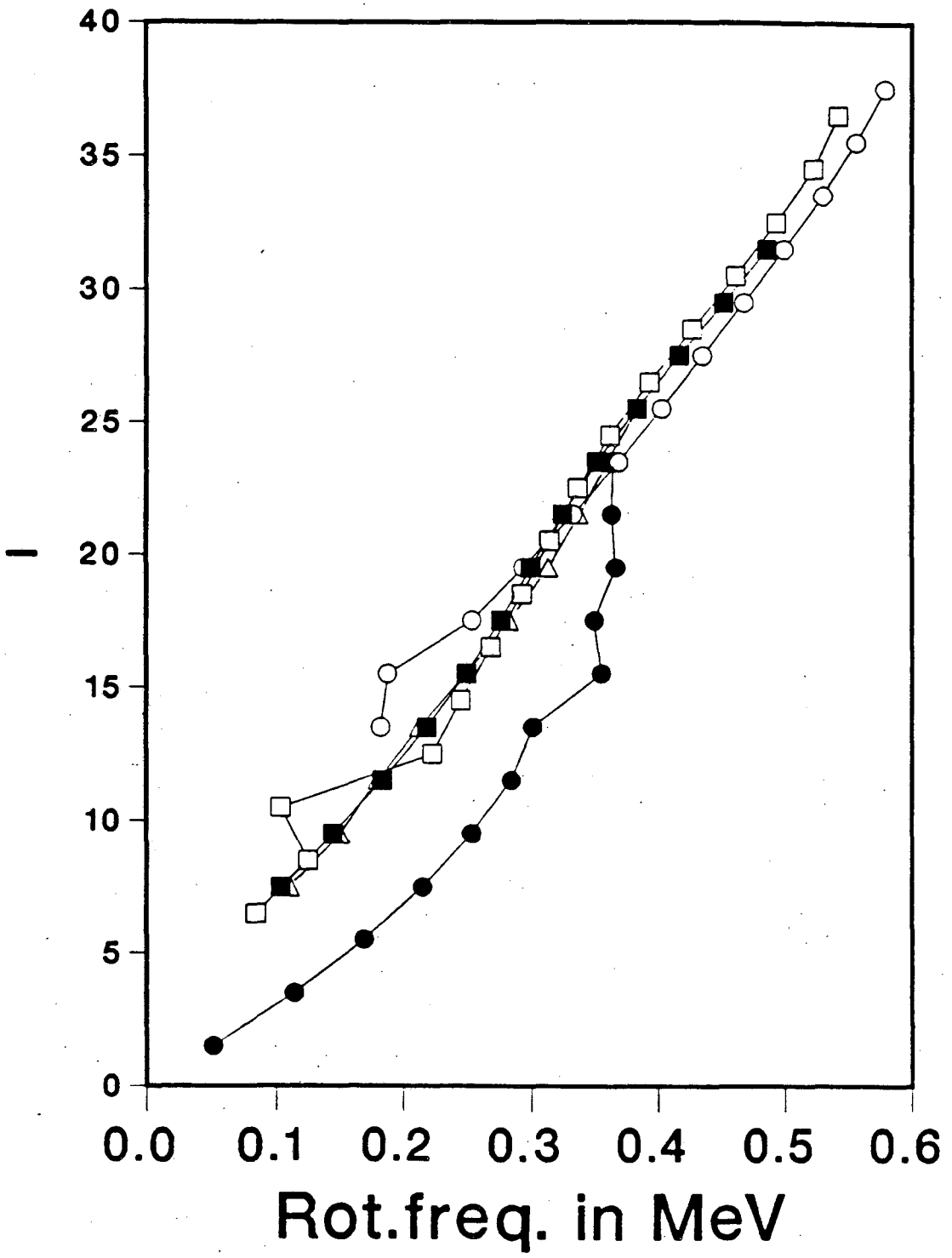

XBL 865-2091A

Fig. 13

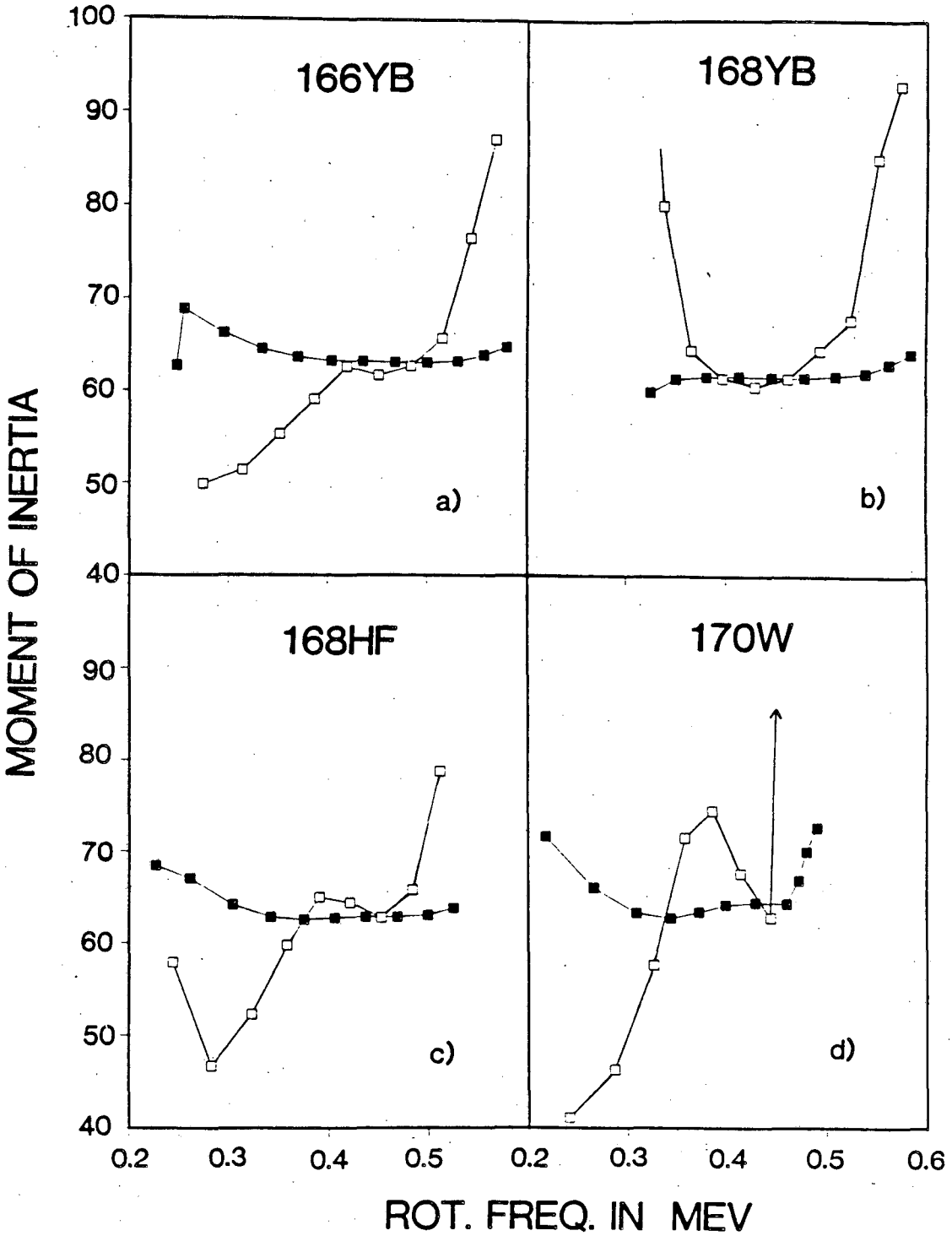
166YB
168YB
168HF
170W
a)
b)
c)
d)
MOMENT OF INERTIA
ROT. FREQ. IN MEV
100
90
80
70
60
50
40
0.2
0.3
0.4
0.5
0.6
XBL 865-2100

Fig. 14

LAWRENCE BERKELEY LABORATORY
TECHNICAL INFORMATION DEPARTMENT
UNIVERSITY OF CALIFORNIA
BERKELEY, CALIFORNIA 94720